Spatiotemporal Variability of Tropical Cyclone Induced Ocean Heat Uptake and Its Effect on Ocean Heat Content

Kaigui Fan [a], Xidong Wang [a,b*], Juan Liu[c], Caixia Shao [a]

[a] *Key Laboratory of Marine Hazards Forecasting, Ministry of Natural Resources, Hohai University, Nanjing 210098, China;*

[b] *Southern Marine Science and Engineering Guangdong Laboratory (Zhuhai), Zhuhai 519000, China;*

[c] *Beijing Institute of Applied Meteorology, Beijing 100029, China*

**Corresponding author*: Xidong Wang, xidong_wang@hhu.edu.cn

Early Online Release: This preliminary version has been accepted for publication in *Journal of Climate*, may be fully cited, and has been assigned DOI 10.1175/JCLI-D-22-0595.1. The final typeset copyedited article will replace the EOR at the above DOI when it is published.

ABSTRACT

Tropical cyclones (TCs) can pump heat downward into the ocean through inducing intense vertical mixing. Many efforts have been made to estimate the TC-induced ocean heat uptake (OHU), but spatiotemporal variability of TC-induced OHU remains unclear. This study estimates the TC-induced OHU, which takes into account the heat loss at the air-sea interface during TC passage compared to previous studies, and investigates the spatiotemporal variability of TC-induced OHU and its potential impacts on ocean heat content (OHC) during the period 1985-2018. It is found that the spatial distribution of OHU is inhomogeneous, with the largest OHU occurring in the Northwest Pacific, and the category 3-5 TCs contribute approximately 51% of total global OHU per year. The annually accumulated TC-induced OHUs in the regional basins exhibit pronounced interannual variability, which is closely related to the TC power dissipation index (PDI). By decomposing PDI into TC intensity, frequency, and duration, we find that the TC characteristics influencing OHU variability vary by basin. Correlation analyses suggest that the interannual variations of OHUs are linked to El Niño-Southern Oscillation (ENSO). In addition, the OHU might have the potential to influence OHC variability, especially in the equatorial eastern Pacific where there are significant positive correlations between the OHU and OHC with lags of 2-6 months. This has an important implication that TC-induced OHU might have potential effects on ENSO evolution.

Accepted for publication in *Journal of Climate*. DOI 10.1175/JCLI-D-22-0595.1.

1. Introduction

Tropical cyclones (TCs) are one of the most severe weather systems associated with strong winds. During TC passage, the intense winds can cause strong vertical velocity shears at the base of the mixed layer in the ocean, partially accounting for the vigorous mixing, which redistributes heat in the vertical direction, thus cools the surface, and warms the subsurface (e.g., Price 1981; Price et al. 1994; D'Asaro et al. 2007). Sea surface cooling is generally dominated by the vertical mixing and secondarily affected by the heat fluxes at the air-sea interface (Price 1981). In the several weeks after the passage of a TC, the surface cold anomaly is gradually restored by anomalous heat fluxes, while the subsurface warm anomaly will persist for a much longer time due to its different restoration processes from the surface (Pasquero and Emanuel 2008; Mei and Pasquero 2012; Bueti et al. 2014; Li and Sriver 2018). Therefore, when the surface cold anomaly is completely recovered to the background conditions, the ocean experiences a net heat uptake (Mei and Pasquero 2012).

Many previous studies have endeavored to estimate TC-induced ocean heat uptake (OHU). Emanuel (2001) estimated the TC-induced OHU of 1.4 ± 0.7 PW in 1996 by using an axisymmetric TC model coupled with a 1-D ocean model. He argued that the TC-induced OHU must be equilibrated by meridional heat transport out of the tropics, and the amount of the TC-induced OHU could account for a large fraction of the observed maximum zonal integrated poleward heat transport. Sriver and Huber (2007) estimated the annual mean TC-induced OHU of 0.26 PW from 2 m air temperature reanalysis and ocean temperature profiles and suggested that ~15% of the maximum zonal integrated poleward heat transport is related to TCs. Sriver et al. (2008) further utilized the satellite-observed sea surface temperature (SST) to calculate the TC-induced OHU with a temporal peak value of 0.6 PW during the period 1998-2006. Zhang et al. (2019) replaced the fixed domain size with the cold wake size for each TC in the calculation and estimated the annual mean TC-induced OHU of 0.48 ± 0.1 PW. Nevertheless, with the deepening of the winter mixed layer, some of the heat will be released into the atmosphere, and only a portion of the heat will be stored in the permanent thermocline. After accounting for the seasonal evolution of the mixed layer, Jansen et al. (2010) found that only

Accepted for publication in *Journal of Climate*. DOI 10.1175/JCLI-D-22-0595.1.

~0.14 PW of TC-induced OHU would remain in the permanent thermocline. Furthermore, TCs could leave footprints on the sea surface height (SSH). Using satellite-observed SSH data, Mei et al. (2013) calculated the annual mean TC-induced OHU of 0.32 ± 0.15 PW by estimating the thermal expansion of seawater in TCs' wakes. Several studies employed Argo floats to quantify the TC-induced OHU by comparing temperature profiles before and after TC passage, which found that the estimated TC-induced OHU is comparable to the results based on satellite-observed SST (e.g., Park et al. 2011; Cheng et al. 2015). A few modelling studies have also attempted to assess the TC-induced OHU, whereas the results differ by their model configurations (e.g., Vincent et al. 2013; Li et al. 2016; Li and Sriver 2018). Overall, the magnitude of the TC-induced OHU estimated by observations and models still remains largely uncertain.

More recent model studies suggested that the TC-induced OHU is not solely transported poleward but also could converge to the Equator (e.g., Jansen and Ferrari 2009; Fedorov et al. 2010; Sriver and Huber 2010; Manucharyan et al. 2011; Scoccimarro et al. 2011; Vincent et al. 2013; Bueti et al. 2014; Li and Sriver 2018). The meridional heat transport is sensitive to the latitudinal distribution of TC-induced mixing. Due to the low level of TC activity in the vicinity of the equator strip, TCs may increase the equatorward heat transport and therefore decrease the poleward heat transport (Jansen and Ferrari 2009). The heat transport to the Equator might have significant effects on tropical climate, especially in the Pacific, where TCs are most active and the magnitude of TC-induced OHU is the greatest. Over the Northwest Pacific (WP), the TC-induced subsurface warm anomaly would be advected to the western boundary by the North Equatorial Current, then transported to the equatorial western Pacific by the Mindanao Current and further carried by the Equatorial Undercurrent or eastward Kelvin and Yanai waves to the equatorial eastern Pacific (Bueti et al. 2014; Li and Sriver 2018). With the resurfacing of the heat elevated by equatorial upwelling, this might have implications for El Niño-Southern Oscillation (ENSO; Bueti et al. 2014). In addition, Fedorov et al. (2010) found that the convergence of TC-induced OHU to the equator caused a permanent positive ENSO phase in the early Pliocene.

Previous estimates of TC-induced OHU from observations mainly focused on the annual

Accepted for publication in *Journal of Climate*. DOI 10.1175/JCLI-D-22-0595.1.

mean amount. However, how the TC-induced OHU varies with time and space has been unclear. In addition, a few modelling studies focused on the spatiotemporal variability of TC-induced OHU, but their findings have not been confirmed by observations (e.g., Vincent et al. 2013; Bueti et al. 2014; Li and Sriver 2018). Hence, this study examines the spatiotemporal variability of TC-induced OHU and their potential impacts on the variability of upper ocean heat content (OHC) using observational data. The rest of this paper is organized as follows. Section 2 introduces the data and the calculation method of TC-induced OHU and OHC. Section 3 presents the sensitivity of OHU to the data and method used. The relationship of the TC-induced OHU with TC characteristics and the spatial variability of OHU are discussed in section 4. Section 5 investigates the interannual variability of OHU over the northern hemisphere (NH), southern hemisphere (SH), and regional basins and its relationship with TC activity. Section 6 explores the potential impacts of TC-induced OHU on OHC, and a summary and discussions are presented in section 7.

2. Data and methods

a. Data

TC best track data, including 6-hourly TC location and 1-minute averaged maximum sustained wind speed for the period 1985-2018, are obtained from the International Best Track Archive for Climate Stewardship (IBTrACS) version 4 (Knapp et al. 2010; https://www.ncdc.noaa.gov/ibtracs/). TCs with intensities of at least 34 knots (i.e., tropical storms) are included in the analysis because tropical depressions might have little effect on OHU at long timescales (Mei et al. 2013). Here TC locations over land are excluded, and TC translation speed is computed over the 12 h period centered on each TC location. Daily optimally interpolated SST with 9 km spatial resolution from Remote Sensing Systems (hereafter: RSS OISST; http://www.remss.com/measurements/sea-surface-temperature/) for the period from June, 2002 to 2018, which merges microwave satellite observations, is used to derive TC-induced SST anomaly (SSTA) because it can provide improved estimates under TC clouds. The National Oceanic and Atmospheric Administration (NOAA) 0.25° Optimum Interpolation SST version 2.1 (hereafter: NOAA OISST; Reynolds et al. 2007) with a longer

Accepted for publication in *Journal of Climate*. DOI 10.1175/JCLI-D-22-0595.1.

time span from September, 1981 onward, which only includes Advanced Very High Resolution Radiometer (AVHRR) observations, is also obtained to extend our analysis. Monthly temperature profiles with a 0.25° horizontal resolution for the period 1985-2018 from the European Center for Medium Range Weather Forecasts (ECMWF) Operational Ocean Reanalysis System 5 (ORAS5; Zuo et al. 2019; https://www.ecmwf.int/en/research/climate-reanalysis/ocean-reanalysis) are used to estimate TC-induced OHU. Monthly oceanic temperature profiles for the period 1985-2018 from the Simple Ocean Data Assimilation (SODA) reanalysis version 3.4.2 (Carton et al. 2018; https://www2.atmos.umd.edu/~ocean/) are also obtained and used to examine the TC-induced OHU based on ORAS5. This dataset has a spatial resolution of 0.5° × 0.5°. Monthly gridded observational temperature profiles at 1° × 1° resolution from the Institute of Atmospheric Physics (IAP; http://www.ocean.iap.ac.cn) are used to estimate OHC and to validate the ORAS5-based OHU. This product has an advantage in sampling error and reproducing the variability on interannual-to-interdecadal timescales (Cheng et al. 2017, 2019). We use hourly heat fluxes with 0.25° × 0.25° spatial resolution from European Center for Medium Range Weather Forecasts Reanalysis 5 (ERA5; Hersbach et al. 2020 https://www.ecmwf.int/en/forecasts/datasets/reanalysis-datasets/era5) to remove net heat flux at the air–sea interface under TCs when calculating TC-induced OHU. The hourly heat fluxes with a spatial resolution of 0.625° × 0.5° obtained from the Modern-Era Retrospective Analysis for Research and Applications, version 2 (MERRA2; Gelaro et al. 2017; https://disc.gsfc.nasa.gov/datasets?project=MERRA-2) are used for comparison with the OHU estimated using ERA5. Monthly time series of Niño 3.4 index is obtained from https://psl.noaa.gov/gcos_wgsp/Timeseries/.

b. Calculation of TC-induced OHU

Before calculating TC-induced OHU, we primarily construct a domain centered on each 6-hourly TC location with a size of 200 km along the TC track and 2600 km across the track. We then build a 10 km × 10 km grid within the domain and linearly interpolate related data onto the grid. The choice of the cross-section width might influence the estimated amount of TC-induced OHU, which will be discussed in section 3d.

Accepted for publication in *Journal of Climate*. DOI 10.1175/JCLI-D-22-0595.1.

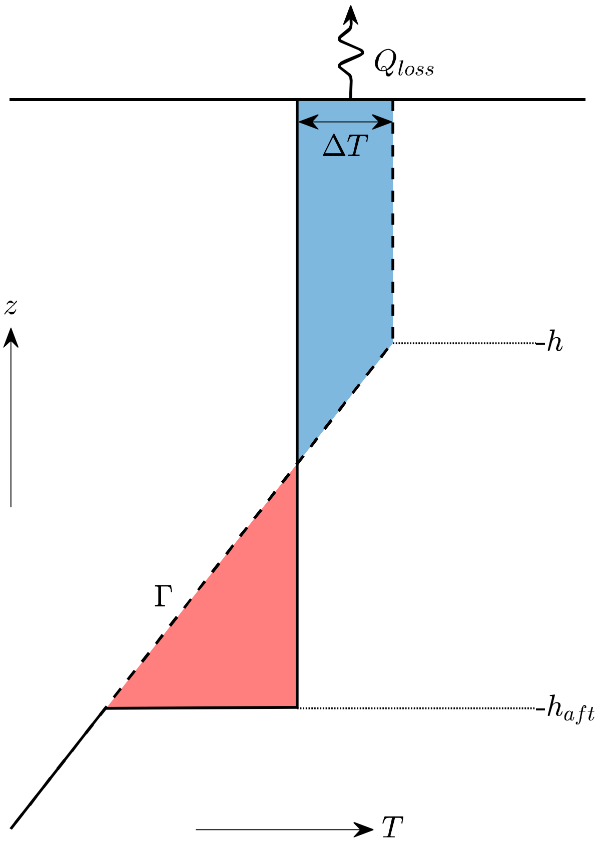

Fig. 1. Schematic diagram of temperature profiles before and after the passage of a TC. The dashed line shows the temperature profile with a mixed layer depth of h in the pre-TC state, and the solid line denotes the temperature profile with a mixed layer depth of h_{aft} in the post-TC state. Γ is the temperature gradient beneath the mixed layer depth. The TC induced surface cooling is ΔT, and the heat loss during the period of TC passage is Q_{loss}. The blue and red patches indicate the cooling and warming, respectively.

In order to estimate the net heat uptake, we assume that the surface cold anomaly is completely restored to pre-TC condition and the subsurface heat uptake is equal to the heat absorbed by the recovery of the surface cold anomaly (Jansen et al. 2010; Fig. 1). Compared to previous estimation methods (e.g., Sriver et al. 2008; Jansen et al. 2010), we further remove the heat loss at the air-sea interface during TC passage from the heat uptake. Then, we can obtain the following equation according to the heat balance,

$$-\Delta T h_{aft} - \frac{\Gamma}{2}\left(h_{aft} - h\right)^2 = \frac{Q_{loss}}{\rho C_p} \tag{1}$$

where ΔT is the TC-induced SSTA, h and h_{aft} are the mixed layer depths in pre- and post-TC states, Γ is the temperature gradient beneath the mixed layer, Q_{loss} is the surface heat loss during

Accepted for publication in *Journal of Climate*. DOI 10.1175/JCLI-D-22-0595.1.

the period of TC passage, ρ is the seawater density, and C_p is the specific heat of seawater. Here ΔT is defined as the difference between the SST 1 day after the TC passage and the average SST for 3 to 10 days before the TC passage. The choice of the SST 1 day after the TC passage is because the SSTA generally peaks at 1 day after the TC passage (Mei and Pasquero 2013). Before computing ΔT, the trend and seasonal cycle have been removed from the satellite-observed SST data. The Γ is derived as a linear fit of the monthly temperature profile from the base of the mixed layer to 50 m below it, and the mixed layer depth is defined as the depth where the temperature decreases 0.2°C compared to the reference depth of 10 m. Although the thickness of seasonal thermocline varies temporally and spatially and is not always 50 m, we chose a fixed depth of 50 m to simplify our calculation. Using different depths (30, 40, 60, and 70 m) to estimate the time series of annually accumulated TC-induced OHU, has minor influence on our results (Figures not shown). The Q_{loss} is the integrated net heat flux from 3 days before TC passage to 1 day after TC passage, which basically covers the signals during TC passage. The ρ and C_p are assigned constant values of 1.02×10^3 kg m^{-3} and 3.9×10^3 J (kg °C)$^{-1}$, respectively (Sriver and Huber 2007).

By solving Eq. (1), the depth of the mixed layer after TC passage h_{aft} can be obtained, and the solution whose value is greater than h is chosen. We then estimate the OHU for each TC location as follows,

$$\begin{gathered} OHU = \int_{w=-1300km}^{w=1300km} \int_{l=-100km}^{l=100km} \rho C_p A(w,l)\, dl dw \\ A(w,l) = \frac{\left[\Gamma\left(h_{aft} - h\right) + \Delta T\right]^2}{2\Gamma} \end{gathered} \tag{2}$$

where A is the area of the warming region indicated by the red patch in Fig.1, and w and l are the cross-track width and along-track length, respectively. If Eq. (1) has no real solution, the $A(w,l)$ of this grid is set to zero. The OHU for each TC location is next averaged over 200 km in the along-track direction and lastly multiplied by half of the distance passed by the TC in 12 h centered on this location. The OHU induced by one TC is calculated by accumulating the heat uptake at each TC location along the TC track, and the annually accumulated OHU is

Accepted for publication in *Journal of Climate*. DOI 10.1175/JCLI-D-22-0595.1.

defined as the sum over the OHU for all TCs that occurred in that year. The annually accumulated OHU is commonly converted to the OHU rate through dividing it by a time period of one year (e.g., Jansen et al. 2010; Mei et al. 2013). To solve the problem of overestimation of OHU due to multiple TCs occurring at close distance and time (i.e., the double-counting problem), we only count one TC location with the higher OHU if the distance between two TC locations that belong to two different TC tracks is shorter than 200 km and the difference between the occurring times of the two locations is less than 5 months (Mei et al. 2013). Using different distances (400, 600, 800, and 1000 km) in the double-counting problem may change the magnitude of annually accumulated OHU, but the temporal evolution of OHU is similar. In order to eliminate the effect of background SST variability on the estimate of OHU, we calculate the background bias by shifting TC tracks one year backward relative to the other datasets. The multi-year average background bias is then obtained by averaging the background bias over all the analyzed years. Finally, the multi-year average background bias is removed from the time series of TC-induced OHU. A more detailed description is presented in section 3d.

c. Calculation of OHC

The monthly OHC in this study is integrated from 700 m depth to the surface,

$$OHC = \int_{-700m}^{0m} \rho C_p T(z)\, dz \tag{3}$$

where T is the temperature, and z is the depth.

3. Sensitivity of OHU to the used data and methods

Under the assumption of Eq. (1), the estimation of TC-induced OHU is jointly affected by satellite-observed SST, air-sea heat fluxes, and subsurface temperature profiles. To clarify whether our estimation is sensitive to the datasets in use, we repeat our estimation by using different datasets listed in section 2a. In addition to the data, the magnitude of the estimated OHU may also be affected by the choice of the cross-section width. Therefore, we analyze the sensitivity of estimation of TC-induced OHU to the used data and method by conducting a series of tests in this section.

Accepted for publication in *Journal of Climate*. DOI 10.1175/JCLI-D-22-0595.1.

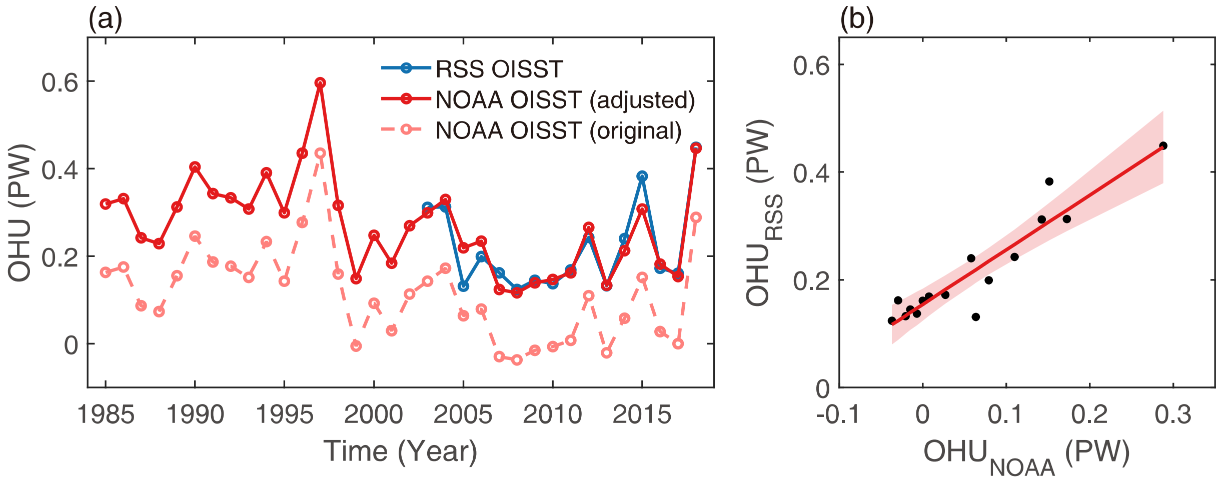

Fig. 2. (a) Time series of TC-induced OHU derived from NOAA OISST (red lines) and RSS OISST (blue line) datasets. The solid and dashed red lines show the adjusted and original OHU estimated from NOAA OISST. The corresponding multi-year average background biases are removed from the time series. (b) Scatterplot between OHU estimated from NOAA OISST and OHU estimated from RSS OISST for the period 2003-2018. Linear fit is denoted as the red line with a 95% confidence interval indicated by shading.

a. Sensitivity of OHU to SST data

Two SST datasets are used to test the sensitivity of the TC-induced OHU estimate in the study. The RSS OISST data combine observations of microwave radiometers, which can lower the uncertainty of measured SST under clouds because of their capability of cloud penetration (Wentz et al. 2000), and RSS OISST data are widely used for TC-related studies (e.g., Fan et al. 2020; Balaguru et al. 2020). We also use the NOAA OISST data, which only include infrared radiometer observations, to get a longer time series of TC-induced OHU. The estimated results are displayed in Fig. 2a. Compared with the OHU estimated from RSS OISST, the NOAA OISST underestimates the OHU as a result of the underestimation of cold wake (Fig. 2a), and there are negative OHU values in some years after removing the multi-year average background biases from the time series. Therefore, we have to correct the OHU time series calculated by NOAA OISST. We find that the OHUs estimated from the two datasets are strongly correlated at 0.94 during 2003-2018 (Fig. 2b). Hence, we could adjust the NOAA OISST estimated OHU by using the linear regression model derived from OHUs estimated from the two datasets during the overlapping period 2003-2018. The adjusted OHU shows the climatology of OHU with a magnitude of ~0.27 PW (~0.22 PW for RSS OISST) which is smaller than previous studies

Accepted for publication in *Journal of Climate*. DOI 10.1175/JCLI-D-22-0595.1.

(e.g., Sriver et al. 2008; Jansen et al. 2010), partly due to the elimination of net heat flux during the TC passage and accounting for the double-counting problem in our analysis, but our estimate still falls within the same uncertainty range as those of previous studies. Although the magnitudes of OHUs estimated by the two SST datasets differ slightly, they show a strong correlation and similar temporal variability over the period 2003-2018.

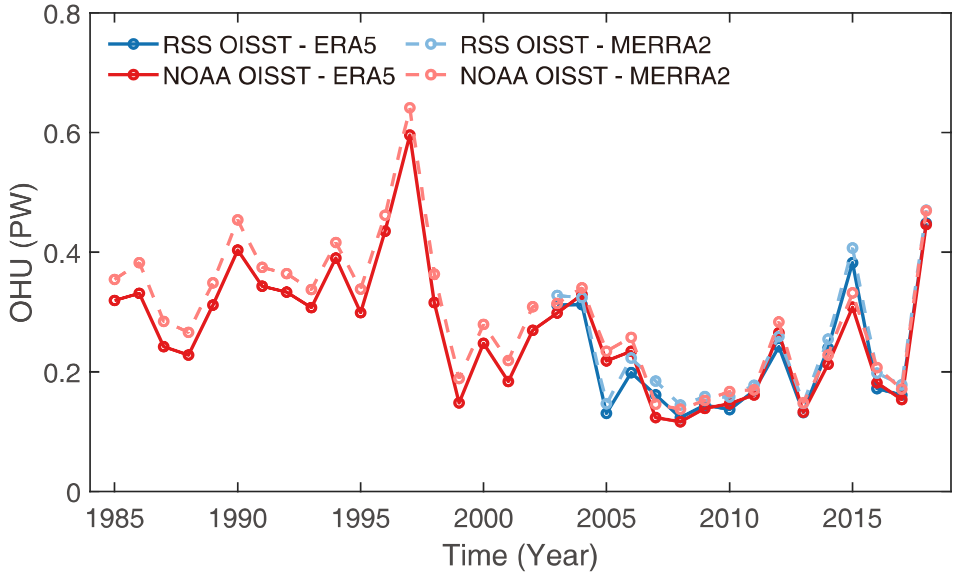

Fig. 3. Time series of TC-induced OHU derived from NOAA OISST (red) and RSS OISST (blue) datasets. The solid and dashed lines indicate that the used heat fluxes are from ERA5 and MERRA2, respectively. The NOAA OISST estimated OHUs are adjusted by using the linear regression model derived from OHUs estimated from the two SST datasets during their overlapping period 2003-2018, and the corresponding multi-year average background biases are removed from the time series.

b. Sensitivity of OHU to heat flux data

The estimate of the TC-induced OHU depends strongly on the magnitude of the cold wake, which is primarily controlled by TC-induced vertical mixing and surface air-sea heat exchange. Vertical mixing is the main contributor to entraining cold water from the thermocline into the mixed layer (e.g., Price 1981; Price et al. 1994; D'Asaro et al. 2007), namely, redistributing heat vertically. The surface heat exchange from ocean to atmosphere generally plays a secondary role in surface cooling. This heat exchange can alter the magnitude of the cold wake but does not directly contribute to the downward heat transport. More importantly, the surface air-sea heat exchange could potentially contribute to more than half of the cold wake magnitude for weak TCs or away from the TC tracks (Vincent et al. 2012b). Hence, the heat exchange

Accepted for publication in *Journal of Climate*. DOI 10.1175/JCLI-D-22-0595.1.

should be eliminated when estimating OHU.

The TC-induced OHUs estimated using ERA5 and MERRA2 are exhibited in Fig. 3. Figure 3 shows that the two datasets have similar performance in estimating the TC-induced OHU. The amount of OHU estimated by MERRA2 is slightly larger than that estimated by ERA5, but this difference is within the range of uncertainty. Moreover, the interannual-to-interdecadal variability of OHU is not sensitive to the heat flux dataset used.

c. Sensitivity of OHU to temperature profile data

The monthly temperature profiles from ORAS5 are used to estimate the mixed layer depth and vertical temperature gradient beneath the mixed layer in the analysis. The dataset assimilates different types of quality-controlled in situ observations and updates the bias correction scheme and quality control method (Zuo et al. 2019). The SODA 3.4.2 oceanic reanalysis and observational temperature data from IAP are used to validate the robustness of the results from ORAS5. The vertical temperature gradient beneath the mixed layer is derived from the linear fit of the temperature profile under the mixed layer. Jansen et al. (2010) found that the results based on the linear fit are close to those estimated by using the quadratic fit. Figure 4 illustrates the temporal evolution of OHUs estimated by using temperature profiles from the three datasets as well as the monthly climatology of ORAS5. The OHUs closely resemble each other in the year-to-year variation, despite slight differences (~10%) in magnitude. Our results suggest that the annually accumulated OHU is not sensitive to the temperature profiles (Fig. 4). Although the temperature gradient could be different before and after TC passage (Wada et al. 2014), we further verified the robustness of our results using the 5-day output of SODA3.7.2 and found that the change in temperature gradient does not substantially influence the annually accumulated OHU (Figures not shown).

Accepted for publication in *Journal of Climate*. DOI 10.1175/JCLI-D-22-0595.1.

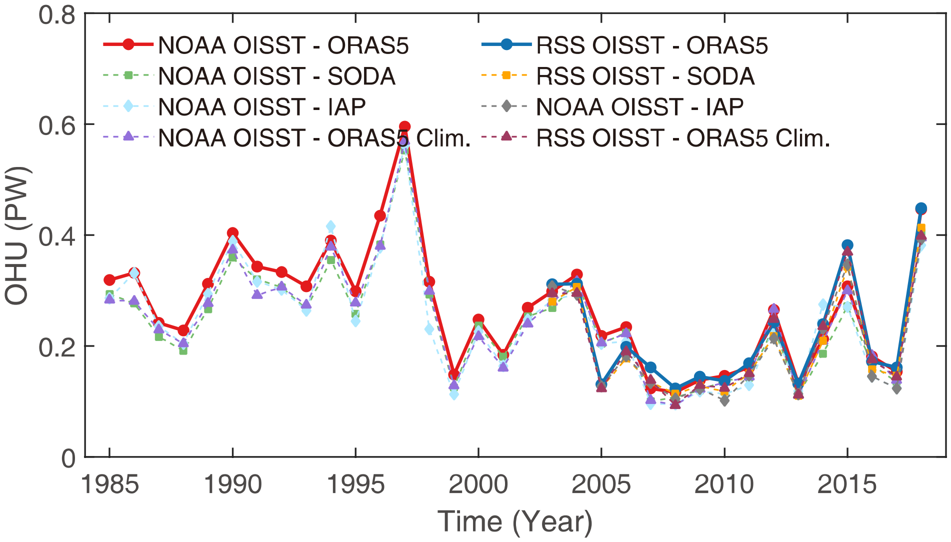

Fig. 4. Time series of TC-induced OHU estimated by using different temperature profile datasets. The thick lines with circles are the OHUs based on ORAS5, the thin dashed lines with squares denote the OHUs based on SODA3.4.2, the thin dashed lines with diamonds show the OHUs based on IAP, and the thin dashed lines with triangles indicate the OHUs based on the monthly climatology of ORAS5. The NOAA OISST estimated OHUs are adjusted by using the linear regression model derived from OHUs estimated from the two SST datasets during their overlapping period 2003-2018, and the corresponding multi-year average background biases are removed from the time series.

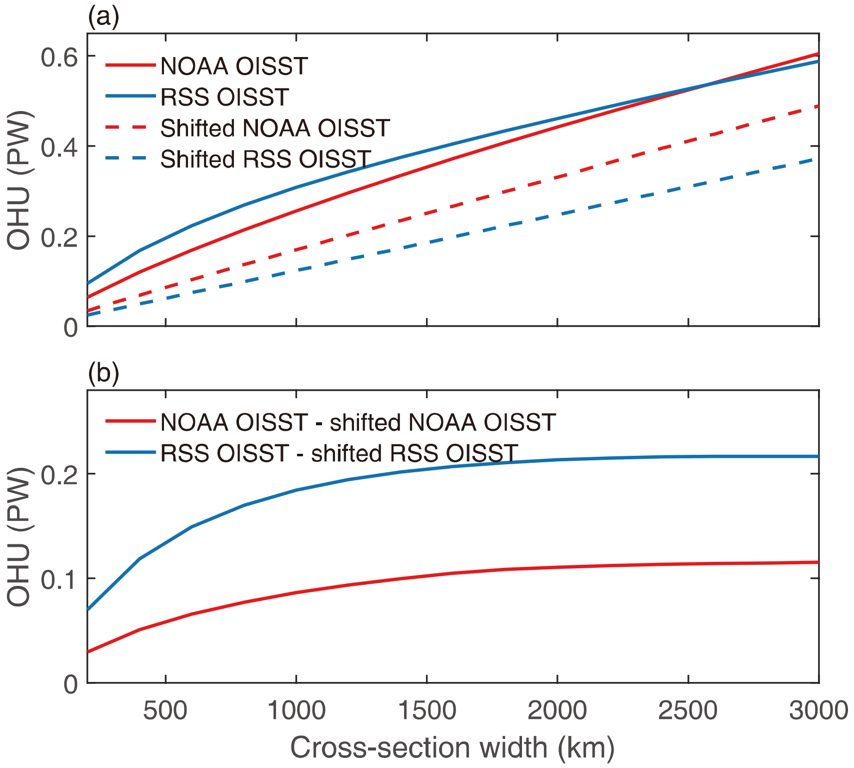

Fig. 5. (a) Climatology of TC-induced OHU varies with the cross-section width. The solid red and blue lines indicate that the OHUs are derived from NOAA OISST and RSS OISST, respectively. The dashed red and blue lines are the multi-year background biases estimated by

Accepted for publication in *Journal of Climate*. DOI 10.1175/JCLI-D-22-0595.1.

using TC best tracks shifted one year backward relative to NOAA OISST and RSS OISST, respectively. (b) Climatology of TC-induced OHU varies with the cross-section width after removing the background biases. The red and blue lines denote that the used SST data are NOAA OISST and RSS OISST, respectively.

d. Sensitivity of OHU to cross-section width

Previous composite analysis has shown that the cold wake size can reach more than 500 km away from the TC track (Mei and Pasquero 2013). Actually, the size of a cold wake is dependent on the characteristics of individual TCs, such as intensity, translation speed, and storm size (Mei and Pasquero 2013; Zhang et al. 2019). The choice of the cold wake size can directly affect the estimation of OHU. Hence, a question arises as to what width of the cross-section is the most appropriate choice to cover the entire cold wake signal. There are several methods documented in the literature. Sriver and Huber (2008) integrated the OHU over a fixed size of $6° \times 6°$ around each TC location. This might underestimate the OHU for those TCs with wider cold wakes. Jansen et al. (2010) utilized a broader width of 15° to remove the bias due to background SST variability by means of shifting TC tracks one or two years relative to SST data. Zhang et al. (2019) recently determined the size of a cold wake by applying two objective methods. In our analysis, we estimate the climatological OHU for various cross-section widths. Figure 5a shows that the climatological OHU initially increases nonlinearly with the cross-section width and then exhibits a nearly linear increase. The shape of the nonlinear increase results from the exponential decay of the cold wake away from its maximum (Price et al. 2008; Dare and McBride 2011). We further estimate the background bias due to background SST variability by shifting TC tracks one year backward relative to the other datasets. For instance, we use the TC tracks data in 1985 combined with SST, heat fluxes, and subsurface temperature data in 1986 to estimate the background bias for 1985. Figure 5a shows that the multi-year average background bias varies linearly with the cross-section width, and the slope is essentially the same as the slope of the linear increase part of the climatological OHU growth curve. This indicates that as the cross-section width increases, an increasing fraction of the estimated OHU is caused by the background SST variability. We then average the background bias over all the analyzed years and remove this multi-year average background bias from the climatology of TC-induced OHU. Figure 5b illustrates that after removing the multi-year average background

Accepted for publication in *Journal of Climate*. DOI 10.1175/JCLI-D-22-0595.1.

bias, the OHU tends to flatten out when the width exceeds 2600 km. We thus conclude that 2600 km is an appropriate width for the cross-section. In addition, although different cross-section widths would affect the magnitude of OHU, they have less impact on the interannual variability of TC-induced OHU.

4. Climatology of TC-induced OHU

It has been widely reported that the magnitude of the TC-induced SST cooling is related to the intensity and translation speed of TCs (e.g., Price 1981; Vincent et al. 2012a,b; Mei and Pasquero 2013). Because a large part of the cooling results from the entrainment of cold thermocline water into the mixed layer, the TC-induced OHU may also be related to the TC characteristics. The TC characteristics vary with region and time, so the TC-induced OHU may differ spatially and temporally. In this section, we explore the dependence of the TC-induced OHU on the TC intensity and translation speed and the spatial variability of the OHU. Due to the low uncertainty of the SST cooling observed by the RSS OISST, our analysis of this section is based on the results derived from the RSS OISST.

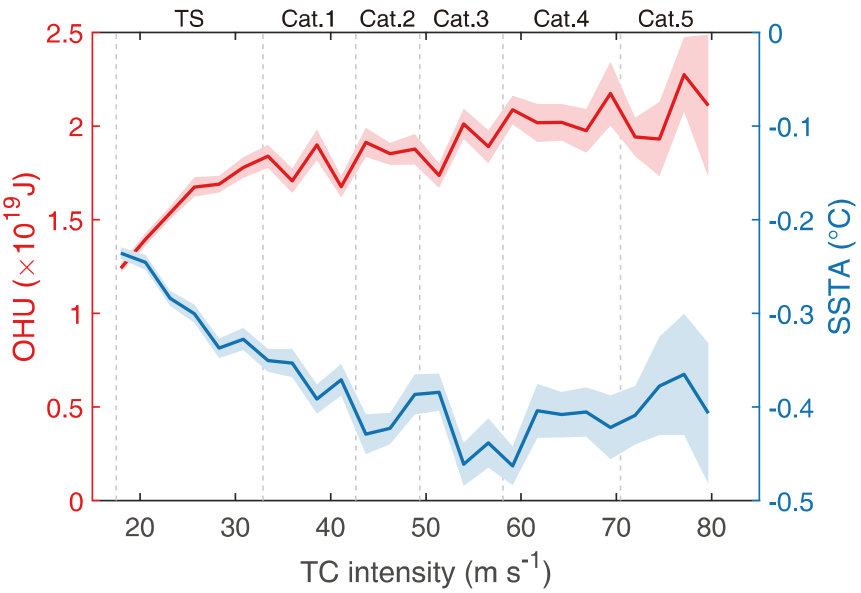

Fig. 6. Distribution of TC-induced OHU and area-mean TC-induced SSTA by TC intensity. Shadings are the standard errors calculated by dividing standard deviation by the square root of sample size. The OHU and SSTA are derived from RSS OISST for the period 2003-2018.

a. Dependence on TC intensity and TC translation speed

Figure 6 shows the relationships between TC-induced OHU, SSTA and intensity. The OHU

Accepted for publication in *Journal of Climate*. DOI 10.1175/JCLI-D-22-0595.1.

increases rapidly with intensity when TCs are in the stage of tropical storms (TSs) and then continues to slowly oscillate upward. The relationship between SSTA and intensity is nearly linear from TSs to category 3 TCs, whereas SSTA does not change significantly with intensity for category 4-5 TCs. We also use various cross-section widths to repeat the calculation to avoid an artificial relationship between OHU and TC intensity, and similar results can be obtained (Fig. S1). The OHU generally increases with the strengthening of the TC intensity, which is consistent with the results of Mei et al. (2013) derived from sea surface height. The stronger TCs tend to induce more intense mixing at the base of the mixed layer, and more heat is transferred downward.

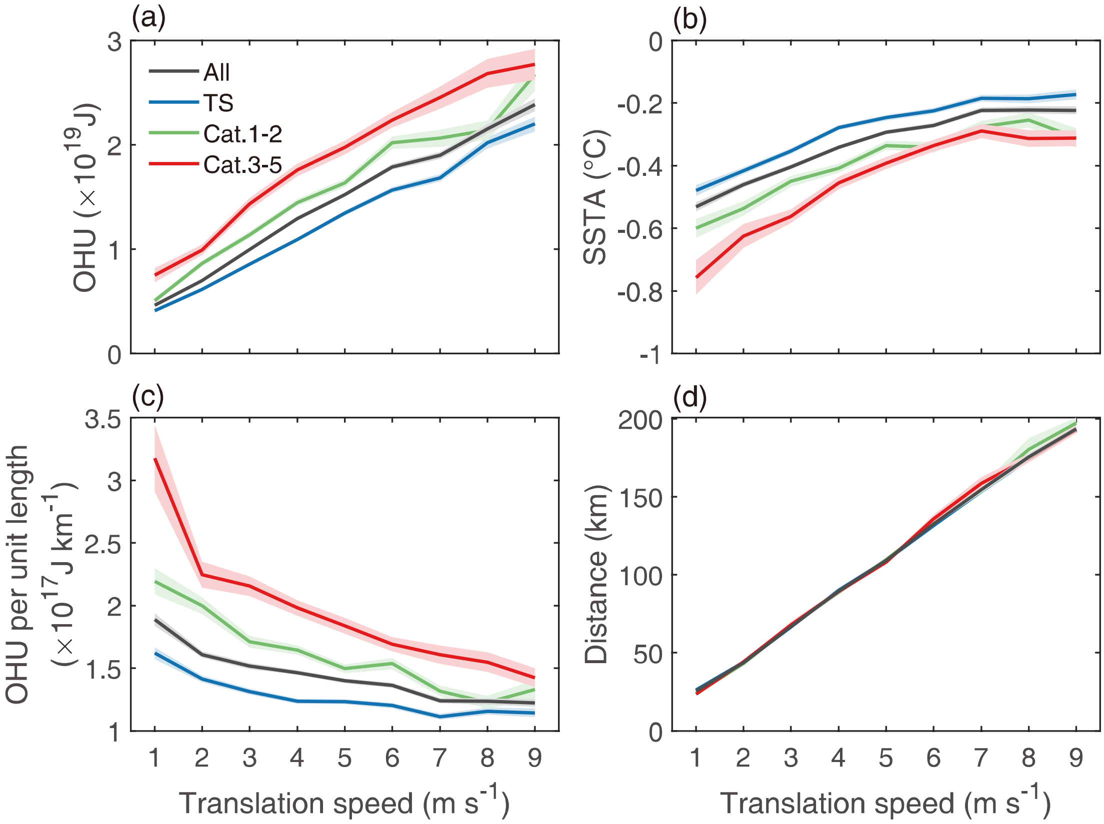

Fig. 7. Distribution of (a) TC-induced OHU, (b) area-mean TC-induced SSTA, (c) TC-induced OHU per unit length of the TC track, and (d) half of the distance passed by the TC in 12 h centered on this location by translation speed of different TC categories. Shadings are the standard errors calculated by dividing standard deviation by the square root of sample size. The OHU and SSTA are derived from RSS OISST for the period 2003-2018.

As is well known, the TC-induced SSTA depends on the TC translation speed (Mei and Pasquero 2013). The same is true for the TC-induced OHU (Fig. 7). On average, a TC with faster a translation speed goes along with a higher OHU (Fig. 7a), and the result still holds for

Accepted for publication in *Journal of Climate*. DOI 10.1175/JCLI-D-22-0595.1.

different cross-section widths (Fig. S2). The relation between OHU and translation speed is the same as the relation between SSTA and translation speed (Fig. 7b). Theoretically, a stronger SSTA comes with a larger OHU. In other words, the relation between OHU and translation speed should be the opposite of the relation between SSTA and translation speed. Figure 7c shows that the relation between the two is indeed the opposite, but instead of OHU it is the OHU per unit length of TC track. The reason for this relation between OHU per unit length of TC track and translation speed is that slow-moving TCs stay longer at a location over the ocean, and thus the upper ocean experiences intense wind-forced mixing for a longer time. As a result, it produces strong cooling at the sea surface and transfers more heat into the subsurface. However, the positive relation between OHU and translation speed primarily arises from the fact that TCs with faster translation speeds can travel longer distances over the ocean (Fig. 7d) and therefore can induce more OHU in the same amount of time.

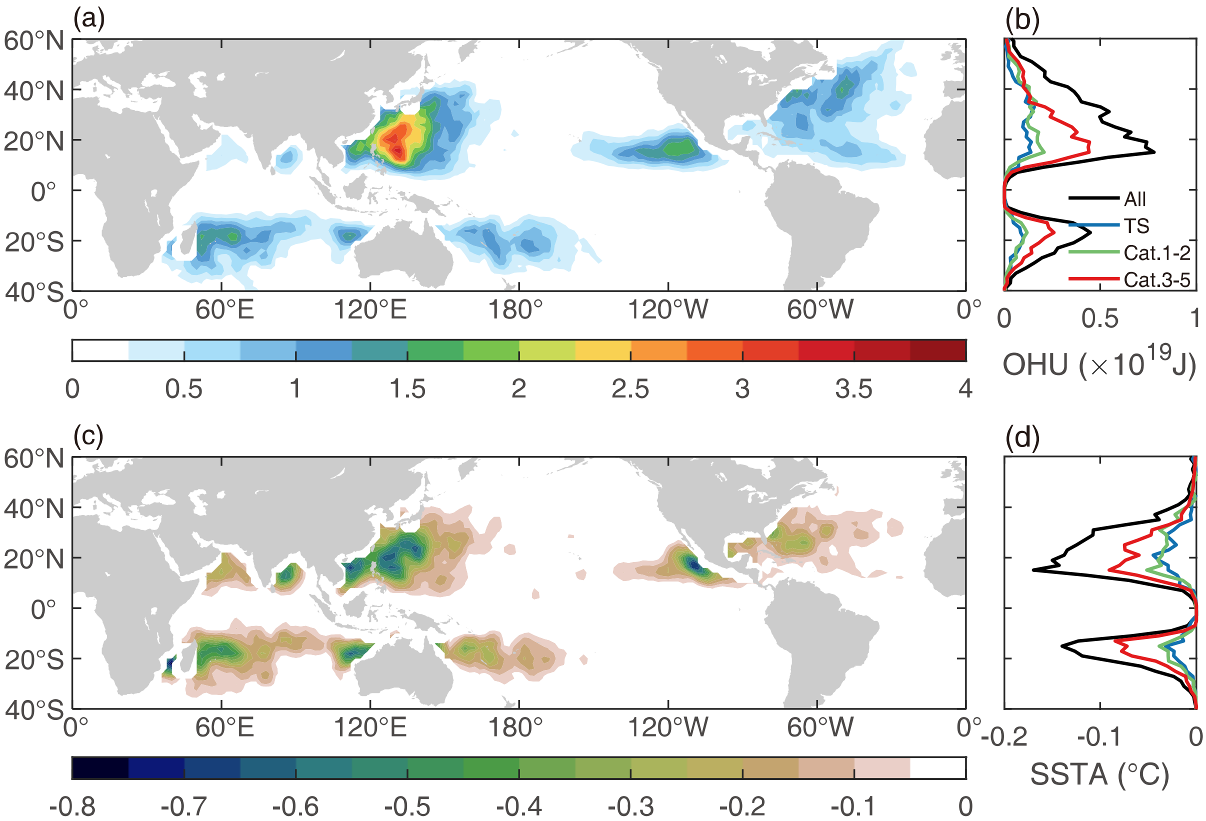

Fig. 8. (a) Annually accumulated TC-induced OHU in each 2° × 2° box. The map is smoothed over a 6° × 6° sliding window. (b) Zonally averaged TSs, category 1-2 TCs (Cat.1-2), category 3-5 TCs (Cat.3-5), and all TCs induced OHU. (c, d) As in (a, b), but for the area-mean TC-induced SSTA. The OHU and SSTA are derived from RSS OISST for the period 2003-2018.

Accepted for publication in *Journal of Climate*. DOI 10.1175/JCLI-D-22-0595.1.

b. Spatial distribution of TC-induced OHU

Figure 8 presents the spatial distribution of the annually accumulated TC-induced OHU and SSTA in each 2° × 2° grid, and the spatial map is smoothed over a 6° × 6° sliding window. The OHU shows a significant inter-basin difference. The WP shows the strongest OHU, peaking at the east of the Philippines. A large OHU center can also be seen in the Northeast Pacific (EP). The OHUs of the North Atlantic (NA) and southern hemisphere (SH) exhibit a polycentric distribution. The inter-basin discrepancy of the TC-induced OHU is substantially related to the geographical distribution of TC frequency (see Fig.3 in Knapp et al. 2010). Therefore, the zonally averaged OHU peaks at ~15°, where most TCs pass over (Fig. 8b). The spatial pattern of the SSTA resembles that of OHU (Fig. 8c and 8d). To test the robustness of the results, we repeated our estimation by utilizing different cross-section widths, and similar patterns can be found except for the magnitude (Fig. S3). As the cross-section width increases, the background bias due to the background SST variability also increases, which leads to an increase in the magnitude of OHU.

We further quantify the contributions of TCs with different categories to the zonally averaged OHU (Fig. 8b and S4). Of interest is that category 3-5 TCs produce ~51% of the total annually accumulated TC-induced OHU, while tropical storms (TSs) and category 1-2 TCs only account for ~22% and ~27% of the total OHU, respectively. The frequency of category 3-5 TCs is only ~30% of the global annual number of TCs, and therefore it confirms that the average OHU induced by strong TCs is larger than that induced by weak TCs. Our results suggest an important role for strong TCs in the TC-induced OHU.

5. Temporal variability of TC-induced OHU

The above analyses showed that the TC-induced OHU varies spatially and with TC characteristics. Owing to the temporal variability of the TC activity, the TC-induced OHU would change with time as well. The RSS OISST can observe the SST responses under TCs because it merges microwave SSTs, and thus its decade-long record provides an opportunity to estimate the temporal variability of the TC-induced OHU. The longer record of NOAA OISST, only combining infrared observations, is taken to extend the analysis. In spite of the

Accepted for publication in *Journal of Climate*. DOI 10.1175/JCLI-D-22-0595.1.

underestimation of the TC-induced OHU by NOAA OISST, the annually accumulated TC-induced OHUs derived from the two SST datasets are strongly correlated during the period 2003-2018. Hence, we conclude that the NOAA OISST could be utilized to estimate the variability of the TC-induced OHU for a longer period. In this section, we mainly focus on the temporal variability of TC-induced OHUs in the NH, SH, and regional basins rather than the magnitude of OHUs.

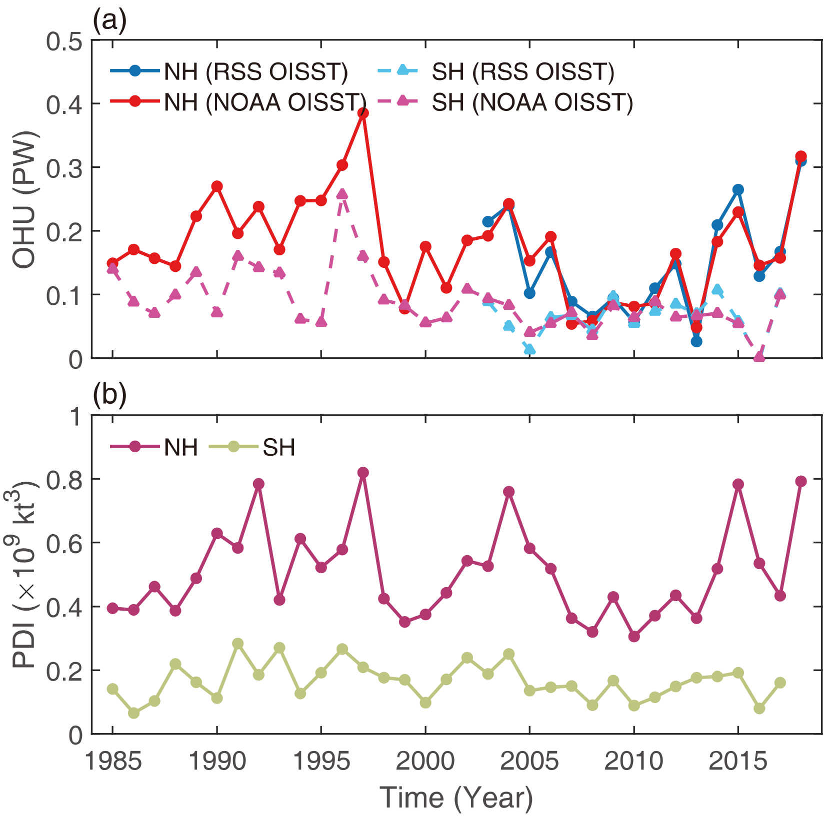

Fig. 9. Time series of (a) TC-induced OHU and (b) PDI for the NH and SH, respectively. The NOAA OISST estimated OHUs are adjusted by using the linear regression model derived from OHUs estimated from the two SST datasets during their overlapping period 2003-2018, and the corresponding multi-year average background biases are removed from the time series. A year in the NH (SH) is defined as January to December (July to June).

a. TC-induced OHU in the NH and SH

Due to the opposite TC seasons in the NH and SH, we analyze the interannual variability of TC-induced OHU in the NH and SH separately. A year in the NH (SH) is defined as January to December (July to June). Figure 9a illustrates the time series of the TC-induced OHU in the NH and SH derived from NOAA OISST and RSS OISST for the period 1985-2018 and 2003-2018, respectively. The OHU in both the NH and SH display marked interannual variability.

Accepted for publication in *Journal of Climate*. DOI 10.1175/JCLI-D-22-0595.1.

The OHU in the NH increases continuously from 1985 to 1997, followed by a sharp decrease in the late 1990s and a quasi-decadal oscillation during 1999-2018, while the OHU in the SH varies with a large amplitude before 1999 and then remains at a relatively stable level after 1999. To understand the influence of TC activity on the interannual variability of the TC-induced OHU, we calculate the power dissipation index (PDI), which is the collective effect of the TC intensity, frequency, and duration, to represent the TC activity. Here the PDI is computed as the sum of the cube of the maximum sustained wind speed during the TC period with an intensity greater than 34 knots over the ocean (Emanuel 2005; Sriver and Huber 2006). The temporal evolution of the PDIs shows a similar pattern to the OHUs (Fig. 9a and 9b), and correlations between the PDIs and the OHUs derived from NOAA OISST and RSS OISST over various periods are markedly significant except that the OHU in the SH derived from RSS OISST is not significantly correlated with PDI (Tables 1 and 2). This indicates that TC activity has a strong impact on OHU variability.

	OHU_{NOAA}		OHU_{RSS}
Period	1985-2018	2003-2018	2003-2018
PDI	**0.83**	**0.91**	**0.87**
N_{TS}	-0.05	-0.03	-0.13
$N_{Cat.1\text{-}2}$	0.29	0.11	-0.02
$N_{Cat.3\text{-}5}$	**0.52**	**0.72**	**0.73**
Intensity	**0.62**	**0.64**	**0.65**
Duration	**0.81**	**0.85**	**0.82**
Translation speed	0.09	0.05	0.08
Tropical SST_{NOAA}	0.20	0.34	0.31
Tropical SST_{RSS}	—	0.41	0.38
Niño 3.4 (ASO)	**0.51**	**0.61**	**0.64**

Table 1. Correlations of the NH TC-induced OHU with PDI, annual TC frequencies of different categories, annual averaged TC intensity, duration, translation speed, detrended tropical SSTs, and Niño 3.4 index, respectively. Significant correlations at the 95% level are in boldface based on the two-tailed Student's t test. The TC characteristics for the NH are computed over January-December. The tropical SST for the NH is calculated by first averaging

Accepted for publication in *Journal of Climate*. DOI 10.1175/JCLI-D-22-0595.1.

over the period January-December and then over a range between 30°S and 30°N. The Niño 3.4 index for the NH is averaged over August-October (ASO).

	OHU_{NOAA}		OHU_{RSS}
Period	1985-2017	2003-2017	2003-2017
PDI	**0.63**	**0.57**	0.43
N_{TS}	**0.36**	-0.37	-0.38
$N_{Cat.1\text{-}2}$	**0.69**	0.51	0.46
$N_{Cat.3\text{-}5}$	0.23	0.36	0.47
Intensity	0.07	0.47	0.46
Duration	**0.65**	**0.57**	0.49
Translation speed	0.09	-0.17	-0.32
Tropical SST_{NOAA}	-0.13	-0.25	-0.11
Tropical SST_{RSS}	—	-0.24	-0.14
Niño 3.4 (JFM)	0.19	0.03	0.20

Table 2. As in Table 1, but for the SH. The TC characteristics for the SH are computed over July-June. The tropical SST for the SH is calculated by first averaging over the period July-June and then over a range between 30°S and 30°N. The Niño 3.4 index for the SH is averaged over January-March (JFM).

Since the PDI is closely connected with the TC-induced OHU and the magnitude of OHU is partly determined by the TC intensity and translation speed, we next attempt to understand the separate contributions of the TC frequency, intensity, duration, and translation speed to the variability of the global TC-induced OHU. The temporal evolutions of TC characteristics in the NH and SH are depicted in Fig. 10. We find that the frequency of category 3-5 TCs has the most pronounced relation with the OHU in the NH (Table 1), while the OHU in the SH seems to have a close relation with the frequency of category 1-2 TCs (Table 2). The annual mean TC intensity and duration show similar interannual variability with the OHU in the NH, and they are both significantly correlated with the OHU (Table 1). Compared to the NH, the OHU in the SH has a stronger correlation with duration (Table 2). The TC translation speeds exhibit strong interannual variability; however, they are not correlated with the TC-induced OHU in the two

Accepted for publication in *Journal of Climate*. DOI 10.1175/JCLI-D-22-0595.1.

hemispheres (Fig. 10, Table 1 and Table 2). Our results show that the interannual variability of OHU in the NH and SH is different, and the TC characteristics that lead to these differences are also different.

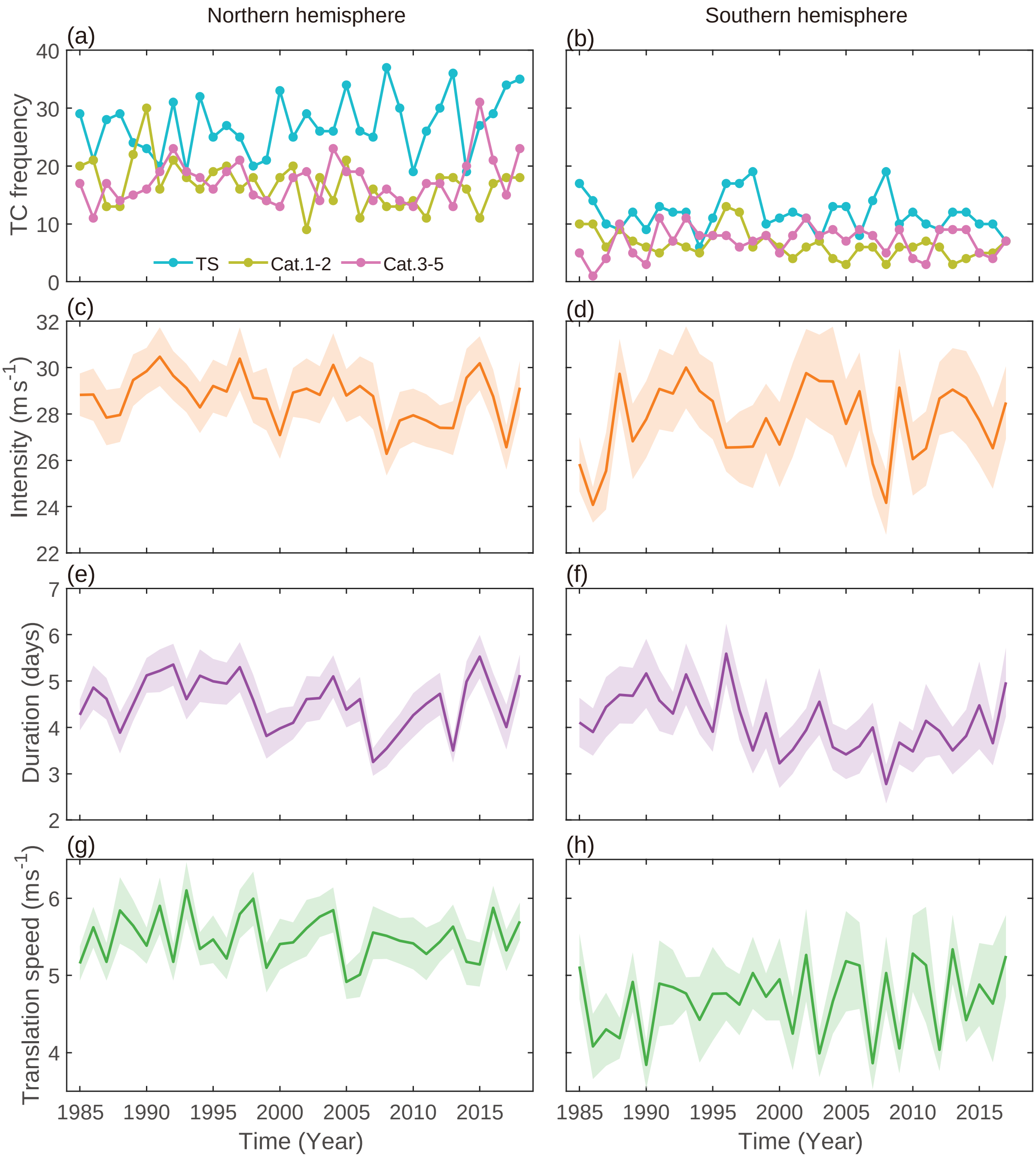

Fig. 10. Temporal evolutions of (a-b) annual frequency of global tropical storms (TS), category 1-2 TCs (Cat.1-2), and category 3-5 TCs (Cat.3-5), (c-b) annual mean TC intensity, (e-f) duration, and (g-h) translation speed for the NH and SH, respectively. The left (right) panels show the TC characteristics in the NH (SH). The annual mean TC intensity, duration, and translation speed are first averaged for each TC and then for all TC globally per year. The year in the NH (SH) is defined as January-December (July-June). Shadings in (c-h) indicate the

Accepted for publication in *Journal of Climate*. DOI 10.1175/JCLI-D-22-0595.1.

standard errors calculated by dividing standard deviation by the square root of sample size.

Earlier studies argued that tropical SST could modulate the PDI (e.g., Emanuel 2005; Sriver and Huber 2006) and further affect the TC-induced OHU (Sriver and Huber 2007). We next examine the role of the tropical SST in the temporal variability of the TC-induced OHU. Since the OHU is estimated separately for the NH and SH, the corresponding tropical SSTs are also averaged over different months. The tropical SST for the NH (SH) is calculated by first averaging over the period January-December (July-June) and then over a range between 30°S and 30°N. Because we mainly pay attention to the interannual variation, the linear trends are removed from tropical SSTs. There is no statistically significant relationship between tropical SST and OHU in either hemisphere (Table 1 and Table 2), suggesting that the interannual variability of OHU is not controlled by tropical SST. Further analysis shows a significant correlation between the OHU in the NH and Niño 3.4 index (Table 1), which infers that the OHU in the NH is sensitive to the equatorial SST rather than the entire tropical SST. The TC-induced OHU in the NH is dominated by the WP (Fig. 8a), and the variability of TC activity in the WP is strongly modulated by ENSO. In the ENSO positive phase, the TC lifetime in the WP tend to be increased (Wang and Chan 2002; Frank and Young 2007), leading to an increase in the annually accumulated TC-induced OHU in the NH. In contrast, there is no significant correlation between OHU in the SH and ENSO (Table 2).

b. TC-induced OHU in regional basins

We further investigate the inter-basin differences in the responses of the TC-induced OHU to TC activity. The time series of the annually accumulated TC-induced OHU derived from NOAA OISST for the WP, EP, NA, North Indian Ocean (NI), South Indian Ocean (SI), and Southwest Pacific (SP) are presented in Fig. 11. The latitude and longitude ranges for the six basins are the same as those in IBTrACS data (Knapp et al. 2010). The negative OHU values in Fig. 11 arise from removing the corresponding multi-year average background biases from the time series. This is to make the sum of the climatological OHUs of different basins consistent with the climatological OHU under global perspective. Figure 11 shows that the interannual variations of TC-induced OHUs in the six basins are quite different. The WP has the largest TC-induced OHU, which accounts for 41% of the global mean TC-induced OHU.

Accepted for publication in *Journal of Climate*. DOI 10.1175/JCLI-D-22-0595.1.

The EP, NA, NI, SI, and SP account for 9%, 12%, 3%, 19%, and 16%, respectively. It is interesting to note that the OHUs in the WP and SI have significant decreasing trends.

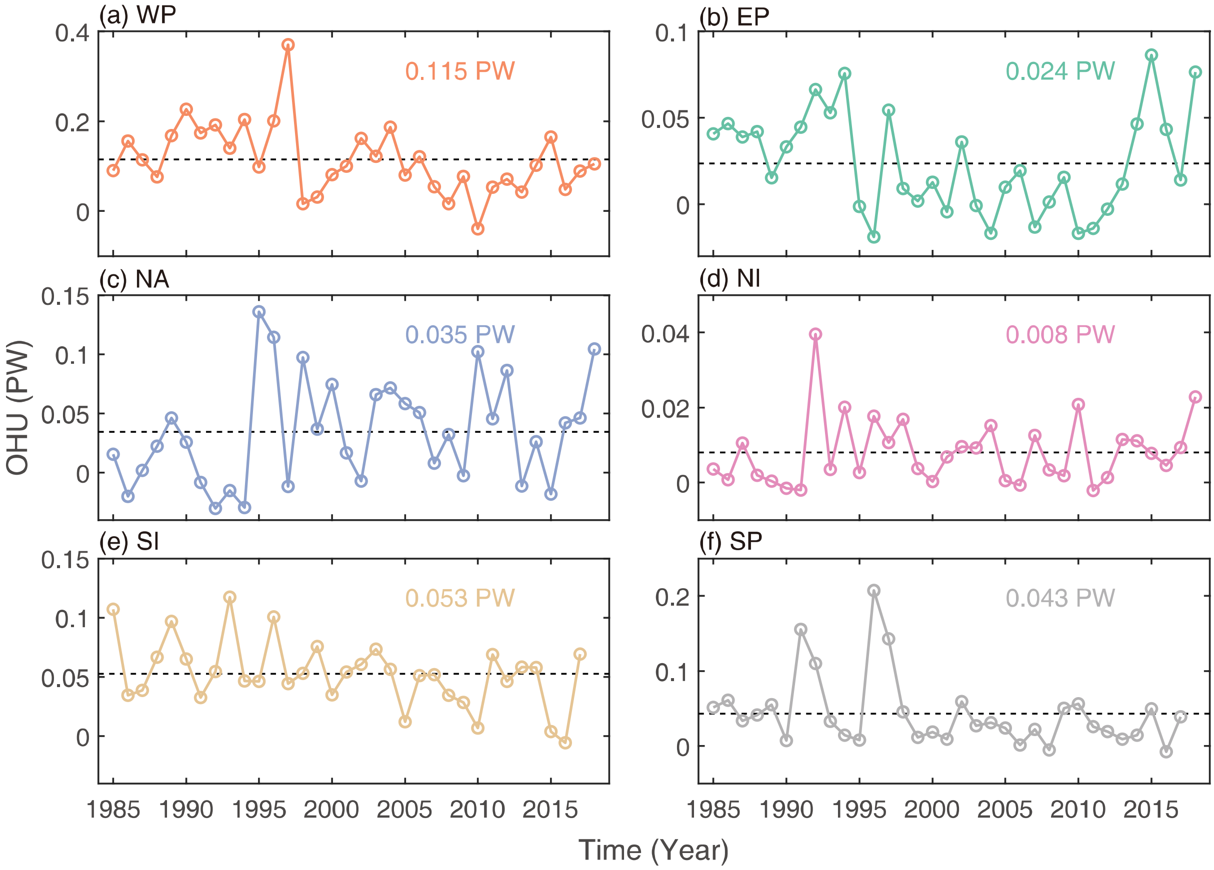

Fig. 11. Time series of the annually accumulated TC-induced OHU estimated from NOAA OISST in the (a) Northwest Pacific (WP), (b) Northeast Pacific (EP), (c) North Atlantic (NA), (d) North Indian Ocean (NI), (e) South Indian Ocean (SI), and (f) Southwest Pacific (SP). Dashed lines denote the mean OHUs, and the specific values are also indicated in each panel. The NOAA OISST estimated OHUs are adjusted by using the linear regression model derived from OHUs estimated from the two SST datasets during their overlapping period 2003-2018, and the corresponding multi-year average background biases are removed from the time series. A year in the WP, EP, NA, and NI (SI and SP) is defined as January to December (July to June).

As with the findings of TC-induced OHUs in the NH and SH, the TC-induced OHUs in all basins have strong correlations with their PDIs. OHUs in the EP and SP have significant correlations with the frequencies of TSs. The frequencies of category 1-2 TCs are correlated with OHUs in all basins except the EP, and the frequencies of category 3-5 TCs have strong connections with the OHUs in the Pacific and Atlantic basins. The averaged TC intensity is significantly correlated with the OHU in the WP, EP, and NA, and their duration has an effect on OHU variability in all six basins (Table 3). Because of the strong modulation of TC activity

Accepted for publication in *Journal of Climate*. DOI 10.1175/JCLI-D-22-0595.1.

by ENSO, we next understand its relationship with the TC-induced OHU (Table 3). We find that the interannual variations of the TC-induced OHU over the three Pacific basins are primarily modulated by ENSO with positive correlations. The TC-induced OHU in the NA is negatively correlated with ENSO. This is because TC activity is suppressed in the NA during the positive ENSO phase (Frank and Young 2007), leading to a unique temporal variation of the TC-induced OHU distinct from the global TC-induced OHU. As for the NI and SI, although plenty of studies have found that the TC activity in the two basins is influenced by ENSO (e.g., Ho et al. 2006; Camargo et al. 2007; Kuleshov et al. 2008; Girishkumar and Ravichandran 2012; Felton et al. 2013; Balaguru et al. 2016; Fan et al. 2019), the variations of TC-induced OHU in these two basins have weak relationships with ENSO.

	WP	EP	NA	NI	SI	SP
PDI	**0.86**	**0.85**	**0.73**	**0.35**	**0.64**	**0.72**
N_{TS}	0.08	**0.38**	0.23	0.24	0.22	**0.47**
$N_{Cat.1\text{-}2}$	**0.57**	0.16	**0.61**	**0.48**	**0.62**	**0.70**
$N_{Cat.3\text{-}5}$	**0.55**	**0.74**	**0.63**	0.31	0.34	**0.44**
Intensity	**0.45**	**0.43**	**0.45**	0.08	0.13	0.17
Duration	**0.74**	**0.51**	**0.69**	**0.42**	**0.58**	**0.48**
Translation speed	-0.04	0.17	0.03	-0.04	0.13	0.12
Niño 3.4	**0.67**	**0.50**	**-0.42**	0.02	-0.21	**0.37**

Table 3. Correlations of TC-induced OHU over regional basins for the period 1985-2018 with regional PDI, annual TC frequencies of different categories, annual mean TC intensity, duration, translation speed, and Niño 3.4 index, respectively. Significant correlations at the 95% level are in boldface based on the two-tailed Student's t test. The TC characteristics for the WP, EP, NA, and NI (SI and SP) are computed over January-December (July-June). Niño 3.4 index is averaged over August-October (ASO) for the WP, EP, and NA, over October-December (OND) for the NI, and over January-March (JFM) for the SI and SP.

6. Potential effects on OHC

A large amount of heat could be consistently pumped downward into the subsurface by TCs annually, which might directly warm the ocean and affect the variability of OHC and even the climate. Here we attempt to understand the potential effect of TC-induced OHU on the

Accepted for publication in *Journal of Climate*. DOI 10.1175/JCLI-D-22-0595.1.

variability of OHC. Figure 12 displays the time series of globally integrated OHC within 0-700 m. It can be seen that the OHC increased persistently during 1985-2018 with a trend of 6.03×10^{21} J yr^{-1}. However, the annually accumulated global TC-induced OHU in the study is ~0.27 PW (corresponding to 8.51×10^{21} J), which suggests that the TC-induced ocean warming is comparable to the observed upper 700 m ocean warming rate (Fig. 12). Figure 12 shows that the amplitude of the temporal variability of OHCA is on the order of 4×10^{22} J, and the maximum monthly accumulated OHU is up to 4×10^{21} J, which indicates that the TC-induced OHU has the ability to account for ~10% of the total OHC variability. Due to the TC-induced inhomogeneous distribution of OHU and heat advection of ocean circulation, it is possible that the OHU may account for the OHC variability in some regions higher than the ratio of OHU to the global OHC variability. Therefore, from the perspective of magnitude, the TC-induced OHU might contribute to the ocean heat budget and might potentially modulate OHC variability.

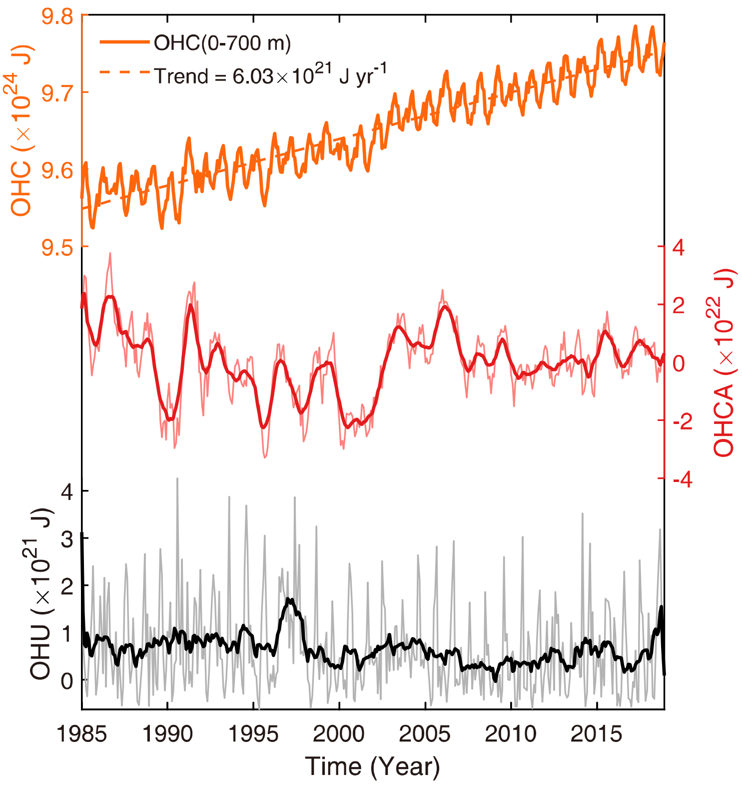

Fig. 12. Time series of monthly global integrated OHC within 0-700 m (solid orange line) along with its trend (dashed orange line), OHC anomaly (OHCA; thin red line) along with its 12-month running mean (thick red line), and monthly accumulated TC-induced OHU (thin gray line) along with its 12-month running mean (thick black line). The seasonal cycle and trend are removed from the OHCA. The NOAA OISST estimated OHU is adjusted by using the linear

Accepted for publication in *Journal of Climate*. DOI 10.1175/JCLI-D-22-0595.1.

regression model derived from OHUs estimated from the two SST datasets during their overlapping period 2003-2018, and the corresponding multi-year average background biases are removed from the time series. The OHU is calculated from IAP data.

Satellite observations and in situ measurements have revealed the net energy imbalance at the top-of-atmosphere, resulting in the excess energy remaining in Earth's system (Loeb et al. 2009, 2012, 2021). The majority of the excess energy is restored in the ocean, increasing the OHC (Loeb et al. 2012, 2021; Cheng et al. 2017). Observations have found that significant trends of upper OHC exist in the 0-700 m and 700-2000 m layers during recent decades (Cheng et al. 2017), and the deep and abyssal oceans also show appreciable warming (Desbruyères et al. 2016). Jansen et al. (2010) suggested that about a quarter of the TC-induced OHU will remain below the permanent thermocline after the deepening of the mixed layer in winter. This part of the OHU might play a role in the deep OHC variability. Therefore, the transient but intense ocean vertical mixing caused by TCs may be one of the processes involved in the downward heat transport into the deep ocean, particularly over the tropical regions.

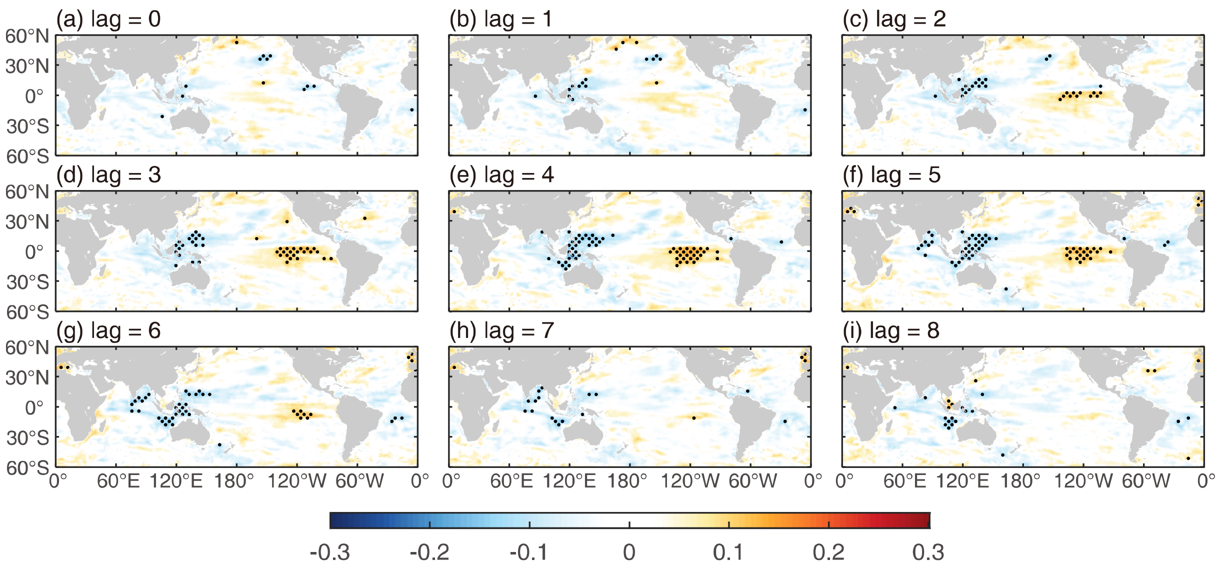

Fig. 13. Maps of the correlation coefficients between monthly accumulated TC-induced OHU in the WP and monthly OHC within 0-700 m with ENSO impact removed. The OHU is calculated from IAP data. Panels (a)-(i) show the correlation coefficients for OHC lagging TC-induced OHU by 0-8 months, respectively. Stippled regions indicate that the correlation is significant at the 95% level.

Accepted for publication in *Journal of Climate*. DOI 10.1175/JCLI-D-22-0595.1.

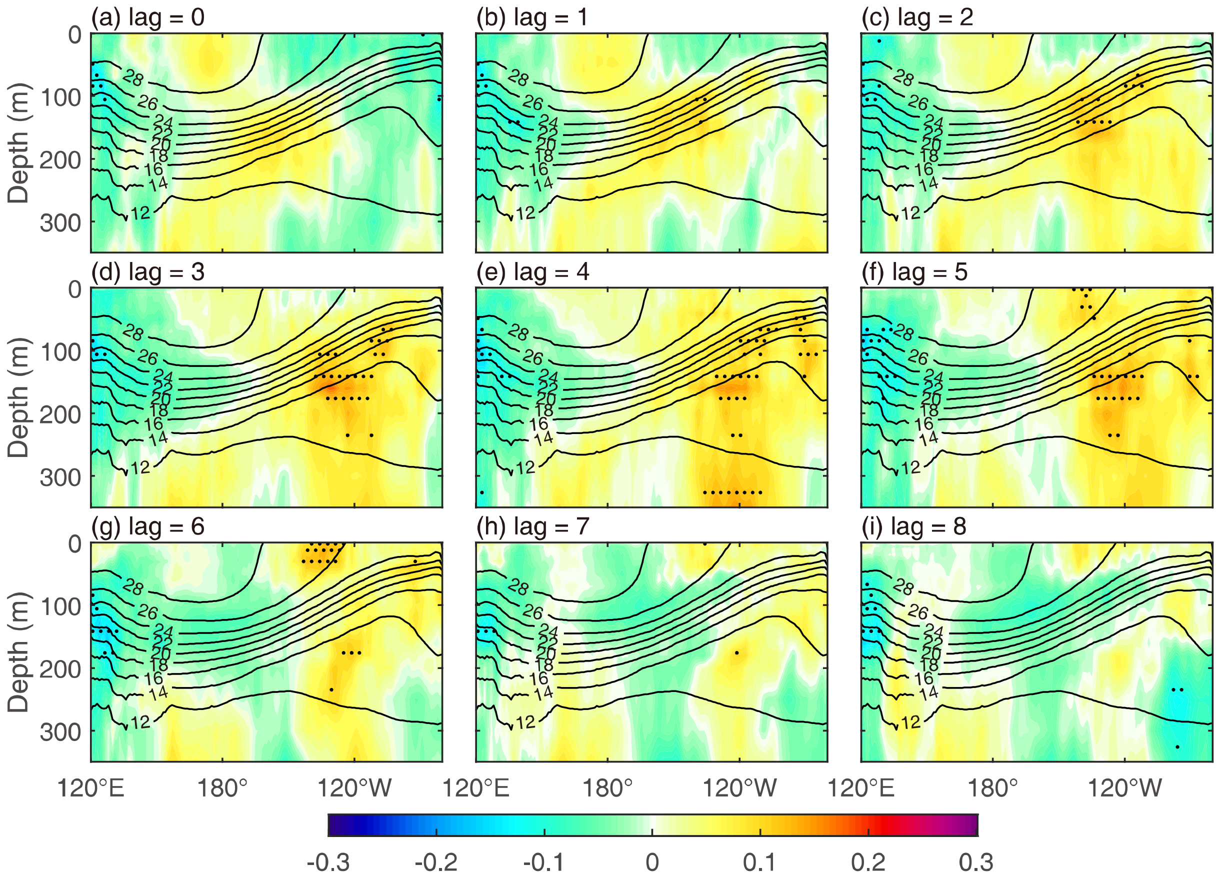

Fig. 14. As in Fig.13, but between the monthly accumulated TC-induced OHU in the WP and the monthly equatorial subsurface temperature averaged over 5°S-5°N with ENSO impact removed. Black lines denote the climatological isotherms.

Because of the strong seasonality in TC activity, the TC-induced OHU also exhibits strong seasonal variability (Fig. 12). Therefore, we further estimate the monthly accumulated TC-induced OHU in the WP, which has the highest OHU among the six basins, and investigate its possible impact on the OHC in the regional oceans. ENSO, as the strongest climate mode, is related to recharge and discharge of OHC in the Pacific Ocean (Jin 1997; Santoso et al. 2017) and has leading and lagging effects on OHC variability (Cheng et al. 2019). Section 5 shows the TC-induced OHU more or less correlating with ENSO. As a result, the TC-induced OHU can be regarded as an intermediate process modulating the OHC variability by ENSO, resulting in the effect of TC-induced OHU on the OHC largely being covered up by ENSO signals. Hence, it is necessary to remove the effect of ENSO from the OHC before analyzing the relationship between the TC-induced OHU and the OHC. The seasonal cycle and trend are first removed from the OHC, and then the leading and lagging effects of ENSO are removed using the method by Werner et al. (2012):

Accepted for publication in *Journal of Climate*. DOI 10.1175/JCLI-D-22-0595.1.

$$OHC_{NOENSO}\left(t\right) = OHC(t) - \sum_{k} b_k \, Niño3.4\left(t-k\right) \tag{4}$$

where OHC and OHC_{NOENSO} are the original OHC and the OHC without ENSO effects, respectively, t is the month in the time series, $k = -8, -7, -6..., 8$ is the lag (negative means lead) month relative to t, and b_k is the regression coefficient on the kth Niño 3.4 predictor. The values of k are set from -8 to 8 because we only explore the relationship for OHC lagging TC-induced OHU by a maximum of 8 months in Fig. 13. After applying this approach, we find no remaining significant correlations between OHC and Niño 3.4 within leads and lags of up to 8 months (Fig. S5), suggesting that the effects of ENSO have been successfully eliminated from the OHC.

Figure 13 shows the correlations between the TC-induced OHU in the WP and the OHC for the upper 700 m after removing the effects of ENSO. The significant positive correlations are distributed along the equatorial eastern Pacific and persist over lag months of 2 to 6 (Fig. 13), which suggests that the TC-induced OHU in the WP could be partly transported to the equatorial eastern Pacific in 2-6 months and thus modulate the equatorial OHC variability. To take a closer look at the effect of WP TCs on the equatorial OHC, we conduct a similar correlation analysis between the TC-induced OHU in the WP and the subsurface temperature averaged over 5°S-5° N. Figure 14 shows that significant positive correlations reside within 300 m in the equatorial eastern Pacific with lags of 2 to 6 months. The significant positive correlations are mainly located in the thermocline at a lag of 2 months and extend below the thermocline at lags of 3 to 5 months. By the lag of 6 months, significant positive correlations are found closer to the sea surface (Fig. 14). Bueti et al. (2014) argued that the TC-induced OHU in the WP is transported to the equatorial eastern Pacific through the pathway of the west Pacific subtropical cell, Mindanao Current, Equatorial Undercurrent, and equatorial waves, and their modelling results showed that the TC-induced OHU could reach the equatorial eastern Pacific in 5 months, which is consistent with our findings.

Accepted for publication in *Journal of Climate*. DOI 10.1175/JCLI-D-22-0595.1.

7. Summary and discussions

In this study, we calculate the TC-induced OHU using the satellite-observed SSTs, subsurface temperature profiles, and air-sea heat fluxes. Compared to previous studies (e.g., Sriver et al. 2008; Jansen et al. 2010), our estimate further takes into account the heat loss at the air-sea interface during TC passage. Based on the estimate, we investigate the spatial and temporal variability of TC-induced OHU in the NH, SH, and regional oceans. Sensitivity tests show that the year-to-year variation of the global TC-induced OHU is not sensitive to the choice of heat fluxes and subsurface temperature profiles datasets. The NOAA OISST, not combining microwave satellite observations, underestimates the magnitude of TC-induced OHU compared to RSS OISST. However, the TC-induced OHUs derived from the two datasets display a similar temporal variation during their overlapping period (2003-2018). The choice of the cross-section width does not substantially change the temporal variation of TC-induced OHU either. Although different cross-section widths would largely change the magnitude of TC-induced OHU, the OHU does not continue to increase when the width exceeds 2600 km after removing the multi-year average background bias. The annual mean TC-induced OHU calculated using the cross-section width of 2600 km also falls within the same uncertainty range as previous studies.

Based on the above results, we use the TC-induced OHU derived from RSS OISST for the period 2003-2018 to analyze the spatial distribution of TC-induced OHU as well as the dependence of OHU on TC intensity and TC translation speed. We further take advantage of the TC-induced OHU estimated from NOAA OISST with a longer period, from 1985 to 2018, to explore its interannual variability in the NH, SH, and regional oceans. It is found that the magnitude of TC-induced OHU increases with the TC intensity and translation speed, but the rate of increase is different. The OHU increases rapidly with TC intensity during the tropical storm stage and shows an oscillatory increase as TCs get stronger. However, the OHU increases almost linearly with the TC translation speed. The linear relationship arises from the fact that TCs with faster translation speeds can travel longer distances over the ocean. The spatial distribution of TC-induced OHU is extremely inhomogeneous, with the largest magnitude of

Accepted for publication in *Journal of Climate*. DOI 10.1175/JCLI-D-22-0595.1.

OHU occurring in the WP. This is substantially related to the geographical distribution of TC frequency, which results in the zonally averaged OHU peaking at ~15°. Of interest is that the category 3-5 TCs are dominant in the TC-induced OHU, accounting for ~51% of the total amount of global TC-induced OHU annually. Previous studies have reported that the TC intensity and ratio of strongest TCs will increase as the climate warms (e.g., Bengtsson et al. 2007; Bender et al. 2010; Bacmeister et al. 2018; Knutson et al. 2020), suggesting a possible increase in TC-induced OHU under a warming scenario. In addition to the TC characteristics, upper ocean thermohaline structure also affects the TC-induced SST cooling (Vincent et al. 2012b), and therefore the TC-induced OHU could be influenced by the oceanic subsurface stratification. Due to the differences in oceanic stratification among basins, the effect of oceanic subsurface stratification on the TC-induced OHU might differ.

The TC-induced OHUs in the NH, SH, and regional basins have significant interannual variability, which strongly correlates with their PDIs. We find that the frequency of category 3-5 TCs, annual mean TC intensity and duration contribute to the OHU variability in the NH, while the same argument does not hold in the SH. Regarding the TC-induced OHUs in the regional oceans, the TC characteristics influencing OHU variability vary by basin. Further correlation analyses show that ENSO is an important climate mode regulating OHU variability. Because of the modulation of ENSO on TC activity, the annually accumulated TC-induced OHU is indirectly influenced by ENSO except in the NI and SI. The TC activity in the NA is below normal during the positive ENSO phase, and thus the TC-induced OHU shows a negative correlation with ENSO, which is different from the other basins.

The TC-induced OHU is not only regulated by climate but might have a potential feedback on climate. From a global perspective, the TC-induced OHU has the ability to account for ~10% of the total OHC variability. However, due to the TC-induced inhomogeneous distribution of OHU and heat advection of ocean circulation, the response of the OHC to OHU could be more pronounced in the regional oceans. One of the most remarkable regions is the equatorial eastern Pacific, where we find significant positive correlations with lags of 2-6 months. It suggests that the TC-induced OHU in the WP might be transported to the equatorial eastern Pacific in 2-6 months. This behavior may have implications for the feedback of TCs on ENSO. Previous

Accepted for publication in *Journal of Climate*. DOI 10.1175/JCLI-D-22-0595.1.

studies have found that the westerly wind bursts are able to boost El Niño, and about 69% of the westerly wind bursts are related to TCs in the WP (Lian et al. 2014, 2018; Chen et al. 2015). The WP TCs can intensify El Niño primarily because they excite the anomalous westerlies and Hadley-like circulation, which weaken the Walker circulation at lower levels and they shallow the thermocline in the tropical western Pacific, while the enhanced equatorial Kelvin waves deepen the thermocline in the tropical eastern Pacific (Wang et al. 2019). These mechanisms are achieved through the dynamic effects of TCs on the atmosphere and ocean. However, the potential impacts of TC-induced OHU on ENSO might provide a possible mechanism imposed by the thermodynamic effects of TCs. Fedorov et al. (2010) showed that the TC-induced OHU could lead to the permanent El Niño in the early Pliocene. In the present climate, the same mechanism might still potentially exert its effects.

In this work, we highlight the temporal variability of the TC-induced OHU in the NH, SH, and regional oceans. However, our estimate is based on the assumption that the surface cold anomaly is completely removed and the OHU balances with the heat absorbed by the recovery of the surface cold anomaly after deducting the heat loss at the air-sea interface during the TC passage. This assumption may not always hold for slow-moving TC locations (translation speed < 3 m s^{-1}), as they may cause strong upwelling, leading to an overestimation of the OHU. We find that the annual mean number of these slow-moving TC locations accounts for ~22% of the total. However, the average contribution of the slow-moving TC locations to the total OHU is only ~8% and ~10% as estimated from NOAA OISST and RSS OISST, respectively. Hence, there is ~10% uncertainty in the OHU caused by slow-moving TC locations. In the real world, the ocean response to TCs is more complicated. As a result, the magnitude of the TC-induced OHU in this study should be taken with caution since it is difficult to accurately estimate the magnitude from observations. Moreover, the OHU magnitude would decrease as the mixed layer deepens in winter (Jansen et al. 2010). With the deepening of the mixed layer, part of the TC-induced OHU will be released into the atmosphere, and the heat remaining in the ocean may be less than our estimate.

Accepted for publication in *Journal of Climate*. DOI 10.1175/JCLI-D-22-0595.1.

Acknowledgements.

The authors are grateful to the providers of the publicly accessible data used in the paper and the three anonymous reviewers for their helpful comments. This study is supported by the Special Founds for Creative Research (2022C61540), the Fundamental Research Funds for the Central Universities (B210203020), the National Natural Science Foundation (41776004, 41876224), and the Opening Project of Key Laboratory of Marine Environmental Information Technology (20195052912). K. Fan is also supported by the Postgraduate Research & Practice Innovation Program of Jiangsu Province (KYCX21_0450) and the scholarship from China Scholarship Council (202106710089).

Data Availability Statement.

The data supporting the findings of this study are openly available. The International Best Track Archive for Climate Stewardship (IBTrACS) version 4 is available at https://www.ncdc.noaa.gov/ibtracs/. The daily optimally interpolated SST data are obtained from Remote Sensing Systems (http://www.remss.com/measurements/sea-surface-temperature/) and NOAA (https://www.ncei.noaa.gov/data/sea-surface-temperature-optimum-interpolation/). The heat flux data are collected from ERA5 (https://www.ecmwf.int/en/forecasts/datasets/reanalysis-datasets/era5) and MERRA2 (https://disc.gsfc.nasa.gov/datasets?project=MERRA-2). The used temperature profile datasets are ORAS5 (https://www.ecmwf.int/en/research/climate-reanalysis/ocean-reanalysis), SODA3.4.2 (https://www2.atmos.umd.edu/~ocean/), and IAP (http://www.ocean.iap.ac.cn/). The monthly Niño 3.4 index is available at https://psl.noaa.gov/gcos_wgsp/Timeseries/.

REFERENCES

Bacmeister, J. T., K. A. Reed, C. Hannay, P. Lawrence, S. Bates, J. E. Truesdale, N. Rosenbloom, and M. Levy, 2018: Projected changes in tropical cyclone activity under future warming scenarios using a high-resolution climate model. *Climatic Change*, **146**, 547–560, https://doi.org/10.1007/s10584-016-1750-x.

Balaguru, K., L. R. Leung, J. Lu, and G. R. Foltz, 2016: A meridional dipole in premonsoon Bay of Bengal tropical cyclone activity induced by ENSO. *J. Geophys. Res. Atmos.*, **121**, 6954–6968, https://doi.org/10.1002/2016JD024936.

——, G. R. Foltz, L. R. Leung, J. Kaplan, W. Xu, N. Reul, and B. Chapron, 2020: Pronounced

Accepted for publication in *Journal of Climate*. DOI 10.1175/JCLI-D-22-0595.1.

impact of salinity on rapidly intensifying tropical cyclones. *Bull. Amer. Meteor. Soc.*, **101**, E1497–E1511, https://doi.org/10.1175/BAMS-D-19-0303.1.

Bender, M. A., T. R. Knutson, R. E. Tuleya, J. J. Sirutis, G. A. Vecchi, S. T. Garner, and I. M. Held, 2010: Modeled impact of anthropogenic warming on the frequency of intense Atlantic hurricanes. *Science*, **327**, 454–458, https://doi.org/10.1126/science.1180568.

Bengtsson, L., K. I. Hodges, M. Esch, N. Keenlyside, L. Kornblueh, J.-J. Luo, and T. Yamagata, 2007: How may tropical cyclones change in a warmer climate? *Tellus A: Dynamic Meteorology and Oceanography*, **59**, 539–561, https://doi.org/10.1111/j.1600-0870.2007.00251.x.

Bueti, M. R., I. Ginis, L. M. Rothstein, and S. M. Griffies, 2014: Tropical cyclone–induced thermocline warming and its regional and global impacts. *J. Climate*, **27**, 6978–6999, https://doi.org/10.1175/JCLI-D-14-00152.1.

Camargo, S. J., K. A. Emanuel, and A. H. Sobel, 2007: Use of a genesis potential index to diagnose ENSO effects on tropical cyclone genesis. *J. Climate*, **20**, 4819–4834, https://doi.org/10.1175/JCLI4282.1.

Carton, J. A., G. A. Chepurin, and L. Chen, 2018: SODA3: A new ocean climate reanalysis. *J. Climate*, **31**, 6967–6983, https://doi.org/10.1175/JCLI-D-18-0149.1.

Chen, D., and Coauthors, 2015: Strong influence of westerly wind bursts on El Niño diversity. *Nature Geosci.*, **8**, 339–345, https://doi.org/10.1038/ngeo2399.

Cheng, L., J. Zhu, and R. L. Sriver, 2015: Global representation of tropical cyclone-induced short-term ocean thermal changes using Argo data. *Ocean Sci.*, **11**, 719–741, https://doi.org/10.5194/os-11-719-2015.

——, K. E. Trenberth, J. Fasullo, T. Boyer, J. Abraham, and J. Zhu, 2017: Improved estimates of ocean heat content from 1960 to 2015. *Sci. Adv.*, **3**, e1601545, https://doi.org/10.1126/sciadv.1601545.

——, ——, J. T. Fasullo, M. Mayer, M. Balmaseda, and J. Zhu, 2019: Evolution of ocean heat content related to ENSO. *J. Climate*, **32**, 3529–3556, https://doi.org/10.1175/JCLI-D-18-

Accepted for publication in *Journal of Climate*. DOI 10.1175/JCLI-D-22-0595.1.

0607.1.

Dare, R. A., and J. L. McBride, 2011: Sea Surface Temperature Response to Tropical Cyclones. *Monthly Weather Review*, **139**, 3798–3808, https://doi.org/10.1175/MWR-D-10-05019.1.

D'Asaro, E. A., T. B. Sanford, P. P. Niiler, and E. J. Terrill, 2007: Cold wake of Hurricane Frances. *Geophys. Res. Lett.*, **34**, L15609, https://doi.org/10.1029/2007GL030160.

Desbruyères, D. G., S. G. Purkey, E. L. McDonagh, G. C. Johnson, and B. A. King, 2016: Deep and abyssal ocean warming from 35 years of repeat hydrography. *Geophys. Res. Lett.*, **43**, 10,356-10,365, https://doi.org/10.1002/2016GL070413.

Emanuel, K., 2001: Contribution of tropical cyclones to meridional heat transport by the oceans. *J. Geophys. Res.*, **106**, 14771–14781, https://doi.org/10.1029/2000JD900641.

——, 2005: Increasing destructiveness of tropical cyclones over the past 30 years. *Nature*, **436**, 686–688, https://doi.org/10.1038/nature03906.

Fan, K., X. Wang, G. R. Foltz, and K. Balaguru, 2019: Meridional oscillation in genesis location of tropical cyclones in the postmonsoon bay of bengal. *Clim. Dyn.*, **53**, 2103–2118, https://doi.org/10.1007/s00382-019-04794-1.

——, ——, and Z. He, 2020: Control of salinity stratification on recent increase in tropical cyclone intensification rates over the postmonsoon Bay of Bengal. *Environ. Res. Lett.*, **15**, 094028, https://doi.org/10.1088/1748-9326/ab9690.

Fedorov, A. V., C. M. Brierley, and K. Emanuel, 2010: Tropical cyclones and permanent El Niño in the early Pliocene epoch. *Nature*, **463**, 1066–1070, https://doi.org/10.1038/nature08831.

Felton, C. S., B. Subrahmanyam, and V. S. N. Murty, 2013: ENSO-modulated cyclogenesis over the Bay of Bengal. *J. Climate*, **26**, 9806–9818, https://doi.org/10.1175/JCLI-D-13-00134.1.

Frank, W. M., and G. S. Young, 2007: The interannual variability of tropical cyclones. *Mon. Wea. Rev.*, **135**, 3587–3598, https://doi.org/10.1175/MWR3435.1.

Accepted for publication in *Journal of Climate*. DOI 10.1175/JCLI-D-22-0595.1.

Gelaro, R., and Coauthors, 2017: The Modern-Era Retrospective Analysis for Research and Applications, Version 2 (MERRA-2). *J. Climate*, **30**, 5419–5454, https://doi.org/10.1175/JCLI-D-16-0758.1.

Girishkumar, M. S., and M. Ravichandran, 2012: The influences of ENSO on tropical cyclone activity in the Bay of Bengal during October-December. *J. Geophys. Res.*, **117**, C02033, https://doi.org/10.1029/2011JC007417.

Hersbach, H., and Coauthors, 2020: The ERA5 global reanalysis. *Q.J.R. Meteorol. Soc.*, **146**, 1999–2049, https://doi.org/10.1002/qj.3803.

Ho, C.-H., J.-H. Kim, J.-H. Jeong, H.-S. Kim, and D. Chen, 2006: Variation of tropical cyclone activity in the South Indian Ocean: El Niño–Southern Oscillation and Madden-Julian Oscillation effects. *J. Geophys. Res.*, **111**, D22101, https://doi.org/10.1029/2006JD007289.

Jansen, M. F., and R. Ferrari, 2009: Impact of the latitudinal distribution of tropical cyclones on ocean heat transport. *Geophys. Res. Lett.*, **36**, L06604, https://doi.org/10.1029/2008GL036796.

——, ——, and T. A. Mooring, 2010: Seasonal versus permanent thermocline warming by tropical cyclones. *Geophys. Res. Lett.*, **37**, L03602, https://doi.org/10.1029/2009GL041808.

Jin, F.-F., 1997: An Equatorial Ocean Recharge Paradigm for ENSO. Part I: Conceptual Model. *J. Atmos. Sci.*, **54**, 811–829, https://doi.org/10.1175/1520-0469(1997)054<0811:AEORPF>2.0.CO;2.

Knapp, K. R., M. C. Kruk, D. H. Levinson, H. J. Diamond, and C. J. Neumann, 2010: The International Best Track Archive for Climate Stewardship (IBTrACS): unifying tropical cyclone data. *Bull. Amer. Meteor. Soc.*, **91**, 363–376, https://doi.org/10.1175/2009BAMS2755.1.

Knutson, T., and Coauthors, 2020: Tropical Cyclones and Climate Change Assessment: Part II: Projected Response to Anthropogenic Warming. *Bulletin of the American Meteorological Society*, **101**, E303–E322, https://doi.org/10.1175/BAMS-D-18-0194.1.

Kuleshov, Y., L. Qi, R. Fawcett, and D. Jones, 2008: On tropical cyclone activity in the Southern

Accepted for publication in *Journal of Climate*. DOI 10.1175/JCLI-D-22-0595.1.

Hemisphere: Trends and the ENSO connection. *Geophys. Res. Lett.*, **35**, L14S08, https://doi.org/10.1029/2007GL032983.

Li, H., and R. L. Sriver, 2018: Impact of tropical cyclones on the global ocean: Results from multidecadal global ocean simulations isolating tropical cyclone forcing. *J. Climate*, **31**, 8761–8784, https://doi.org/10.1175/JCLI-D-18-0221.1.

——, ——, and M. Goes, 2016: Modeled sensitivity of the Northwestern Pacific upper-ocean response to tropical cyclones in a fully coupled climate model with varying ocean grid resolution. *J. Geophys. Res. Oceans*, **121**, 586–601, https://doi.org/10.1002/2015JC011226.

Lian, T., D. Chen, Y. Tang, and Q. Wu, 2014: Effects of westerly wind bursts on El Niño: A new perspective. *Geophys. Res. Lett.*, **41**, 3522–3527, https://doi.org/10.1002/2014GL059989.

——, ——, ——, X. Liu, J. Feng, and L. Zhou, 2018: Linkage between westerly wind bursts and tropical cyclones. *Geophys. Res. Lett.*, **45**, https://doi.org/10.1029/2018GL079745.

Loeb, N. G., B. A. Wielicki, D. R. Doelling, G. L. Smith, D. F. Keyes, S. Kato, N. Manalo-Smith, and T. Wong, 2009: Toward optimal closure of the Earth's top-of-atmosphere radiation budget. *J. Climate*, **22**, 748–766, https://doi.org/10.1175/2008JCLI2637.1.

——, J. M. Lyman, G. C. Johnson, R. P. Allan, D. R. Doelling, T. Wong, B. J. Soden, and G. L. Stephens, 2012: Observed changes in top-of-the-atmosphere radiation and upper-ocean heating consistent within uncertainty. *Nature Geosci.*, **5**, 110–113, https://doi.org/10.1038/ngeo1375.

——, G. C. Johnson, T. J. Thorsen, J. M. Lyman, F. G. Rose, and S. Kato, 2021: Satellite and ocean data reveal marked increase in Earth's heating rate. *Geophys. Res. Lett.*, **48**, https://doi.org/10.1029/2021GL093047.

Manucharyan, G. E., C. M. Brierley, and A. V. Fedorov, 2011: Climate impacts of intermittent upper ocean mixing induced by tropical cyclones. *J. Geophys. Res.*, **116**, C11038, https://doi.org/10.1029/2011JC007295.

Mei, W., and C. Pasquero, 2012: Restratification of the upper ocean after the passage of a

Accepted for publication in *Journal of Climate*. DOI 10.1175/JCLI-D-22-0595.1.

tropical cyclone: A numerical study. *J. Phys. Oceanogr.*, **42**, 1377–1401, https://doi.org/10.1175/JPO-D-11-0209.1.

——, and ——, 2013: Spatial and temporal characterization of sea surface temperature response to tropical cyclones. *J. Climate*, **26**, 3745–3765, https://doi.org/10.1175/JCLI-D-12-00125.1.

——, F. Primeau, J. C. McWilliams, and C. Pasquero, 2013: Sea surface height evidence for long-term warming effects of tropical cyclones on the ocean. *Proc. Natl. Acad. Sci.*, **110**, 15207–15210, https://doi.org/10.1073/pnas.1306753110.

Park, J. J., Y.-O. Kwon, and J. F. Price, 2011: Argo array observation of ocean heat content changes induced by tropical cyclones in the north Pacific. *J. Geophys. Res.*, **116**, C12025, https://doi.org/10.1029/2011JC007165.

Pasquero, C., and K. Emanuel, 2008: Tropical cyclones and transient upper-ocean warming. *J. Climate*, **21**, 149–162, https://doi.org/10.1175/2007JCLI1550.1.

Price, J. F., 1981: Upper ocean response to a hurricane. *J. Phys. Oceanogr.*, **11**, 153–175, https://doi.org/10.1175/1520-0485(1981)011<0153:UORTAH>2.0.CO;2.

——, T. B. Sanford, and G. Z. Forristall, 1994: Forced stage response to a moving hurricane. *J. Phys. Oceanogr.*, **24**, 233–260, https://doi.org/10.1175/1520-0485(1994)024<0233:FSRTAM>2.0.CO;2.

——, J. Morzel, and P. P. Niiler, 2008: Warming of SST in the cool wake of a moving hurricane. *J. Geophys. Res.*, **113**, C07010, https://doi.org/10.1029/2007JC004393.

Reynolds, R. W., T. M. Smith, C. Liu, D. B. Chelton, K. S. Casey, and M. G. Schlax, 2007: Daily high-resolution-blended analyses for sea surface temperature. *J. Climate*, **20**, 5473–5496, https://doi.org/10.1175/2007JCLI1824.1.

Santoso, A., M. J. Mcphaden, and W. Cai, 2017: The Defining Characteristics of ENSO Extremes and the Strong 2015/2016 El Niño. *Rev. Geophys.*, **55**, 1079–1129, https://doi.org/10.1002/2017RG000560.

Scoccimarro, E., and Coauthors, 2011: Effects of tropical cyclones on ocean heat transport in a

Accepted for publication in *Journal of Climate*. DOI 10.1175/JCLI-D-22-0595.1.

high-resolution coupled general circulation model. *J. Climate*, **24**, 4368–4384, https://doi.org/10.1175/2011JCLI4104.1.

Sriver, R. L., and M. Huber, 2006: Low frequency variability in globally integrated tropical cyclone power dissipation. *Geophys. Res. Lett.*, **33**, 2006GL026167, https://doi.org/10.1029/2006GL026167.

——, and ——, 2007: Observational evidence for an ocean heat pump induced by tropical cyclones. *Nature*, **447**, 577–580, https://doi.org/10.1038/nature05785.

——, and ——, 2010: Modeled sensitivity of upper thermocline properties to tropical cyclone winds and possible feedbacks on the Hadley circulation. *Geophys. Res. Lett.*, **37**, https://doi.org/10.1029/2010GL042836.

——, ——, and J. Nusbaumer, 2008: Investigating tropical cyclone-climate feedbacks using the TRMM Microwave Imager and the Quick Scatterometer. *Geochem. Geophys. Geosyst.*, **9**, Q09V11, https://doi.org/10.1029/2007GC001842.

Vincent, E. M., M. Lengaigne, G. Madec, J. Vialard, G. Samson, N. C. Jourdain, C. E. Menkes, and S. Jullien, 2012a: Processes setting the characteristics of sea surface cooling induced by tropical cyclones. *J. Geophys. Res.*, **117**, C02020, https://doi.org/10.1029/2011JC007396.

——, ——, J. Vialard, G. Madec, N. C. Jourdain, and S. Masson, 2012b: Assessing the oceanic control on the amplitude of sea surface cooling induced by tropical cyclones. *J. Geophys. Res.*, **117**, C05023, https://doi.org/10.1029/2011JC007705.

——, G. Madec, M. Lengaigne, J. Vialard, and A. Koch-Larrouy, 2013: Influence of tropical cyclones on sea surface temperature seasonal cycle and ocean heat transport. *Clim. Dyn.*, **41**, 2019–2038, https://doi.org/10.1007/s00382-012-1556-0.

Wada, A., T. Uehara, and S. Ishizaki, 2014: Typhoon-induced sea surface cooling during the 2011 and 2012 typhoon seasons: observational evidence and numerical investigations of the sea surface cooling effect using typhoon simulations. *Prog. Earth Planet. Sci.*, **1**, 11, https://doi.org/10.1186/2197-4284-1-11.

Wang, B., and J. C. L. Chan, 2002: How Strong ENSO Events Affect Tropical Storm Activity

Accepted for publication in *Journal of Climate*. DOI 10.1175/JCLI-D-22-0595.1.

over the Western North Pacific*. *J. Climate*, **15**, 1643–1658, https://doi.org/10.1175/1520-0442(2002)015<1643:HSEEAT>2.0.CO;2.

Wang, Q., and Coauthors, 2019: Tropical cyclones act to intensify El Niño. *Nat. Commun.*, **10**, 3793, https://doi.org/10.1038/s41467-019-11720-w.

Wentz, F. J., C. Gentemann, D. Smith, and D. Chelton, 2000: Satellite measurements of sea surface temperature through clouds. *Science*, **288**, 847–850, https://doi.org/10.1126/science.288.5467.847.

Werner, A., A. M. Maharaj, and N. J. Holbrook, 2012: A new method for extracting the ENSO-independent Indian Ocean Dipole: application to Australian region tropical cyclone counts. *Clim. Dyn.*, **38**, 2503–2511, https://doi.org/10.1007/s00382-011-1133-y.

Zhang, J., Y. Lin, D. R. Chavas, and W. Mei, 2019: Tropical cyclone cold wake size and its applications to power dissipation and ocean heat uptake estimates. *Geophys. Res. Lett.*, **46**, 10177–10185, https://doi.org/10.1029/2019GL083783.

Zuo, H., M. A. Balmaseda, S. Tietsche, K. Mogensen, and M. Mayer, 2019: The ECMWF operational ensemble reanalysis–analysis system for ocean and sea ice: a description of the system and assessment. *Ocean Sci.*, **15**, 779–808, https://doi.org/10.5194/os-15-779-2019.

Accepted for publication in *Journal of Climate*. DOI 10.1175/JCLI-D-22-0595.1.